LETTER

doi:10.1038/nature10831

Experimental adaptation of an influenza H5 HA confers respiratory droplet transmission to a reassortant H5 HA/H1N1 virus in ferrets

Masaki Imai[1], Tokiko Watanabe[1,2], Masato Hatta[1], Subash C. Das[1], Makoto Ozawa[1,3], Kyoko Shinya[4], Gongxun Zhong[1], Anthony Hanson[1], Hiroaki Katsura[5], Shinji Watanabe[1,2], Chengjun Li[1], Eiryo Kawakami[2], Shinya Yamada[5], Maki Kiso[5], Yasuo Suzuki[6], Eileen A. Maher[1], Gabriele Neumann[1] & Yoshihiro Kawaoka[1,2,3,5]

Highly pathogenic avian H5N1 influenza A viruses occasionally infect humans, but currently do not transmit efficiently among humans. The viral haemagglutinin (HA) protein is a known host-range determinant as it mediates virus binding to host-specific cellular receptors[1–3]. Here we assess the molecular changes in HA that would allow a virus possessing subtype H5 HA to be transmissible among mammals. We identified a reassortant H5 HA/H1N1 virus—comprising H5 HA (from an H5N1 virus) with four mutations and the remaining seven gene segments from a 2009 pandemic H1N1 virus—that was capable of droplet transmission in a ferret model. The transmissible H5 reassortant virus preferentially recognized human-type receptors, replicated efficiently in ferrets, caused lung lesions and weight loss, but was not highly pathogenic and did not cause mortality. These results indicate that H5 HA can convert to an HA that supports efficient viral transmission in mammals; however, we do not know whether the four mutations in the H5 HA identified here would render a wholly avian H5N1 virus transmissible. The genetic origin of the remaining seven viral gene segments may also critically contribute to transmissibility in mammals. Nevertheless, as H5N1 viruses continue to evolve and infect humans, receptor-binding variants of H5N1 viruses with pandemic potential, including avian–human reassortant viruses as tested here, may emerge. Our findings emphasize the need to prepare for potential pandemics caused by influenza viruses possessing H5 HA, and will help individuals conducting surveillance in regions with circulating H5N1 viruses to recognize key residues that predict the pandemic potential of isolates, which will inform the development, production and distribution of effective countermeasures.

Although H5N1 viruses continue to cause outbreaks in poultry and there are cases of human infection in Indonesia, Vietnam, Egypt and elsewhere (http://www.who.int/influenza/human_animal_interface/H5N1_cumulative_table_archives/en/index.html), they have not acquired the ability to cause human-to-human transmission. Investment in H5N1 vaccines has therefore been questioned. However, because humans lack immunity to influenza viruses possessing an H5 HA, the emergence of a transmissible H5-HA-possessing virus would probably cause a pandemic. To prepare better for such a scenario, it is critical that we understand the molecular changes that may render H5-HA-possessing viruses transmissible in mammals. Such knowledge would allow us to monitor circulating or newly emerging variants for their pandemic potential, focus eradication efforts on viruses that already have acquired subsets of molecular changes critical for transmission in mammals, stockpile antiviral compounds in regions where such viruses circulate, and initiate vaccine generation and large-scale production before a pandemic. Therefore, we studied the molecular features that would render H5-HA-possessing viruses transmissible in mammals.

Previous studies suggested that HA has a major role in host-range restriction of influenza A viruses[1–3]. The HA of human isolates preferentially recognizes sialic acid linked to galactose by α2,6-linkages (Siaα2,6Gal), whereas the HA of avian isolates preferentially recognizes sialic acid linked to galactose by α2,3-linkages (Siaα2,3Gal)[3]. A small number of avian H5N1 viruses isolated from humans show limited binding to human-type receptors, a property conferred by several amino acid changes in HA[4–9]. None of the H5N1 viruses tested transmitted efficiently in a ferret model[10–13], although, while our paper was under review, one study[14] reported that a virus with a mutant H5 HA and a neuraminidase (NA) of a human virus in the H5N1 virus background caused respiratory droplet transmission in one of two contact ferrets.

To identify novel mutations in avian H5 HAs that confer human-type receptor-binding preference, we introduced random mutations into the globular head (amino acids 120–259 (H3 numbering), which includes the receptor-binding pocket) of A/Vietnam/1203/2004 (H5N1; VN1203) HA (Supplementary Fig. 1). Although this virus was isolated from a human, its HA retains avian-type receptor-binding properties[6,15]. We also replaced the multibasic HA cleavage sequence with a non-virulent-type cleavage sequence, allowing us to perform studies in biosafety level 2 containment (http://www.who.int/csr/resources/publications/influenza/influenzaRMD2003_5.pdf). The mutated polymerase chain reaction (PCR) products were cloned into RNA polymerase I plasmids[16] containing the VN1203 HA complementary DNA, which resulted in *Escherichia coli* libraries representing the randomly generated HA variants. Sequence analysis of 48 randomly selected clones indicated an average of 1.0 amino acid changes per HA globular head (data not shown). To generate an H5N1 virus library, plasmids for the synthesis of the mutated HA gene and the unmodified NA gene of VN1203 were transfected into human embryonic kidney (293T) cells together with plasmids for the synthesis of the six remaining viral genes of A/Puerto Rico/8/34 (H1N1; PR8), a laboratory-adapted human influenza A virus.

Turkey red blood cells (TRBCs; which possess both Siaα2,6Gal and Siaα2,3Gal on their surface (data not shown)) were treated with *Salmonella enterica* serovar Typhimurium LT2 sialidase, which preferentially removes α2,3-linked sialic acid (that is, avian-type receptors), creating TRBCs that predominantly possess Siaα2,6Gal on the cell surface (Siaα2,6-TRBCs; Supplementary Fig. 2). The virus library was then adsorbed to Siaα2,6-TRBCs at 4 °C and extensively washed to remove nonspecifically or weakly bound viruses. Bound viruses were eluted by incubation at 37 °C for 30 min, and then diluted to approximately ~0.5 viruses per well (on the basis of a pilot experiment that

[1]Department of Pathobiological Sciences, University of Wisconsin-Madison, Madison, Wisconsin 53711, USA. [2]ERATO Infection-Induced Host Responses Project, Saitama 332-0012, Japan. [3]Department of Special Pathogens, International Research Center for Infectious Diseases, Institute of Medical Science, University of Tokyo, Tokyo 108-8639, Japan. [4]Department of Microbiology and Infectious Diseases, Kobe University, Hyogo 650-0017, Japan. [5]Division of Virology, Department of Microbiology and Immunology, Institute of Medical Science, University of Tokyo, Tokyo 108-8639, Japan. [6]Health Science Hills, College of Life and Health Sciences, Chubu University, Kasugai, Aichi 487-8501, Japan.

assessed the approximate number of eluted viruses). We screened one-third of the library (that is, 2.1×10^6 viruses) in three separate selection experiments (that is, 0.7×10^6 viruses per experiment) and isolated 370 viruses that bound to Siaα2,6-TRBCs (Supplementary Fig. 2). Individual viruses were then grown in Madin-Darby canine kidney (MDCK) cells modified to overexpress Siaα2,6Gal (AX4 cells[17]), and screened again for their ability to agglutinate Siaα2,6-TRBCs (Supplementary Fig. 2). The parental control virus (designated VN1203/PR8) with avian-type receptor-binding specificity agglutinated untreated TRBCs (which possess both human- and avian-type receptors on their surface), but not TRBCs possessing predominantly human-type receptors (Siaα2,6-TRBCs; Supplementary Table 1). By contrast, of the 370 viruses originally isolated, nine agglutinated Siaα2,6-TRBCs, albeit with different efficiencies (Supplementary Table 1). All nine viruses possessed mutations in the region targeted for random mutagenesis; one mutant also possessed an additional mutation (E119G) in an area that was not targeted for mutation. Most of the mutations clustered around the receptor-binding pocket (Fig. 1a). Several of the selected viruses possessed mutations known to increase binding to human-type receptors, including N186K (ref. 9), S227N (ref. 5) and Q226L (which confers human-type receptor binding together with G228S)[15] (all shown in blue in Fig. 1a). The identification of known determinants of human-type receptor-binding specificity from a library of random mutants validates our approach. Notably, our screen also identified mutations not previously associated with receptor-binding specificity.

Although viruses were diluted to ~0.5 viruses per well for amplification in AX4 cells, we cannot exclude the possibility that some wells were infected with more than one virus, resulting in mixed populations. To confirm the significance of the identified mutations in HA for human-type receptor binding, the mutations were engineered into a VN1203/PR8 virus (possessing an avirulent HA cleavage site sequence, as described earlier). All nine mutants were generated; however, after two passages in MDCK cells, the S136N mutation reverted to the wild-type sequence. This mutant was excluded from further evaluation.

First, we confirmed the binding of the remaining eight variants to Siaα2,6-TRBCs (Supplementary Table 1). For comparison, we included a VN1203/PR8 virus with two changes in its HA (Q226L and G228S) previously shown to have increased binding to Siaα2,6Gal[6,15]. Indeed, compared to the wild-type VN1203/PR8 virus, the Q226L/G228S mutant displayed an increased ability to bind to human-type receptors. For the recreated variants, haemagglutination titres were higher and slightly different from the initial characterization, which we attribute to biological differences (the initial characterization was carried out with non-concentrated cell culture supernatant and potentially mixed virus populations, whereas the recreated viruses were concentrated and purified) and to experimental differences (that is, differences between the TRBC batches or the efficiency of α2,3-sialidase treatment, or both). Collectively, however, these experiments demonstrate that this random mutagenesis approach allows the identification of hitherto unrecognized amino acid substitutions that permit avian virus HAs to bind to human-type receptors.

To characterize further the receptor-binding properties of the selected variants, we used solid-phase binding assays in which sialylglycopolymers were absorbed to plates, which were then incubated with virus (Fig. 2a). A virus possessing the HA and NA genes of the seasonal human A/Kawasaki/173/2001 (H1N1; K173) virus and the remaining genes from PR8 (K173/PR8) served as a control virus with typical human-type receptor specificity. Indeed, K173/PR8 preferentially bound to Siaα2,6Gal. In contrast, VN1203/PR8 bound to only Siaα2,3Gal. As reported elsewhere[6,15], the Q226L/G228S mutations led to increased binding to Siaα2,6Gal. Variants I202T/R220S, W153R/T160I, N169I/H184L/I217M and H130Q/K157E resembled VN1203/PR8 in their binding to glycans, despite the fact that these mutants weakly agglutinated Siaα2,6-TRBCs (see Supplementary Table 1). These viruses may have bound to glycans on TRBCs that were different from Siaα2,6Galβ1,4GlcNAc used in this study. However, variants N186K/M230I, S227N/G228A and Q226L/E231G showed an appreciable increase in binding to Siaα2,6Gal but also retained binding capacity for Siaα2,3Gal. Of all of the variants tested, only E119G/V152I/N224K/Q226L exhibited specificity for only Siaα2,6Gal. Thus, only one H5 HA variant with receptor-binding capability akin to that of seasonal influenza viruses was isolated from the library screen of 2.1×10^6 viruses. To identify the amino acid change(s) responsible for the conversion from Siaα2,3Gal to Siaα2,6Gal recognition in the E119G/V152I/N224K/Q226L virus HA, we tested the amino acid changes at positions 119, 152, 224 and 226 individually and in various combinations. Solid-phase binding assays demonstrated that the N224K/Q226L combination is critical for the shift from Siaα2,3Gal to Siaα2,6Gal recognition (Fig. 2b); Q226L in combination with V152I also conferred weak binding to α2,6-glycans.

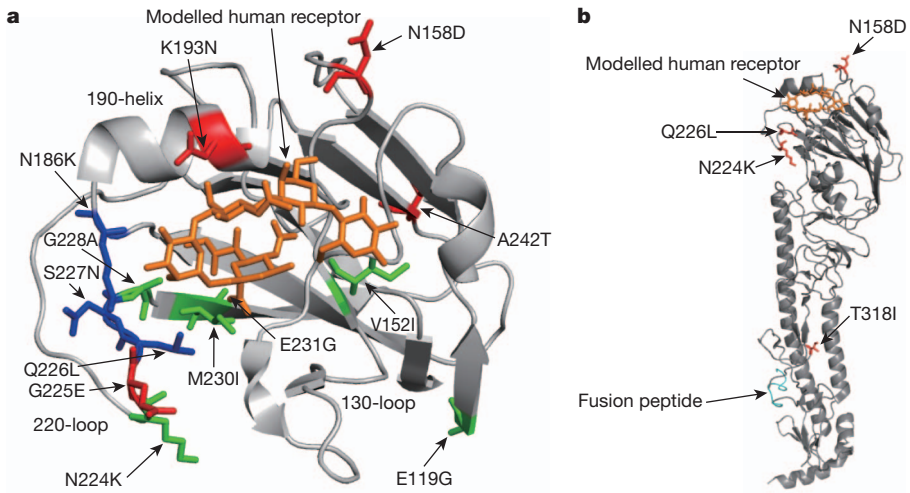

Figure 1 | Localization of amino acid changes identified in this study on the three-dimensional structure of the monomer of VN1203 HA (Protein Data Bank accession 2FK0)[15]. a, Close-up view of the globular head of VN1203 HA. Mutations known to increase affinity to human-type receptors are shown in blue. Amino acid changes not previously known to affect receptor binding are shown in green. Additional mutations that occurred in the HA of H5 avian–human reassortant viruses during replication and/or transmission in ferrets are shown in red. **b**, The positions of four mutations in the HA of H5 transmissible reassortant mutant virus, HA(N158D/N224K/Q226L/T318I)/CA04, are highlighted in red. The fusion peptide of HA is shown in cyan. All mutations are shown with H3 numbering. Images were created with MacPymol (http://www.pymol.org/).

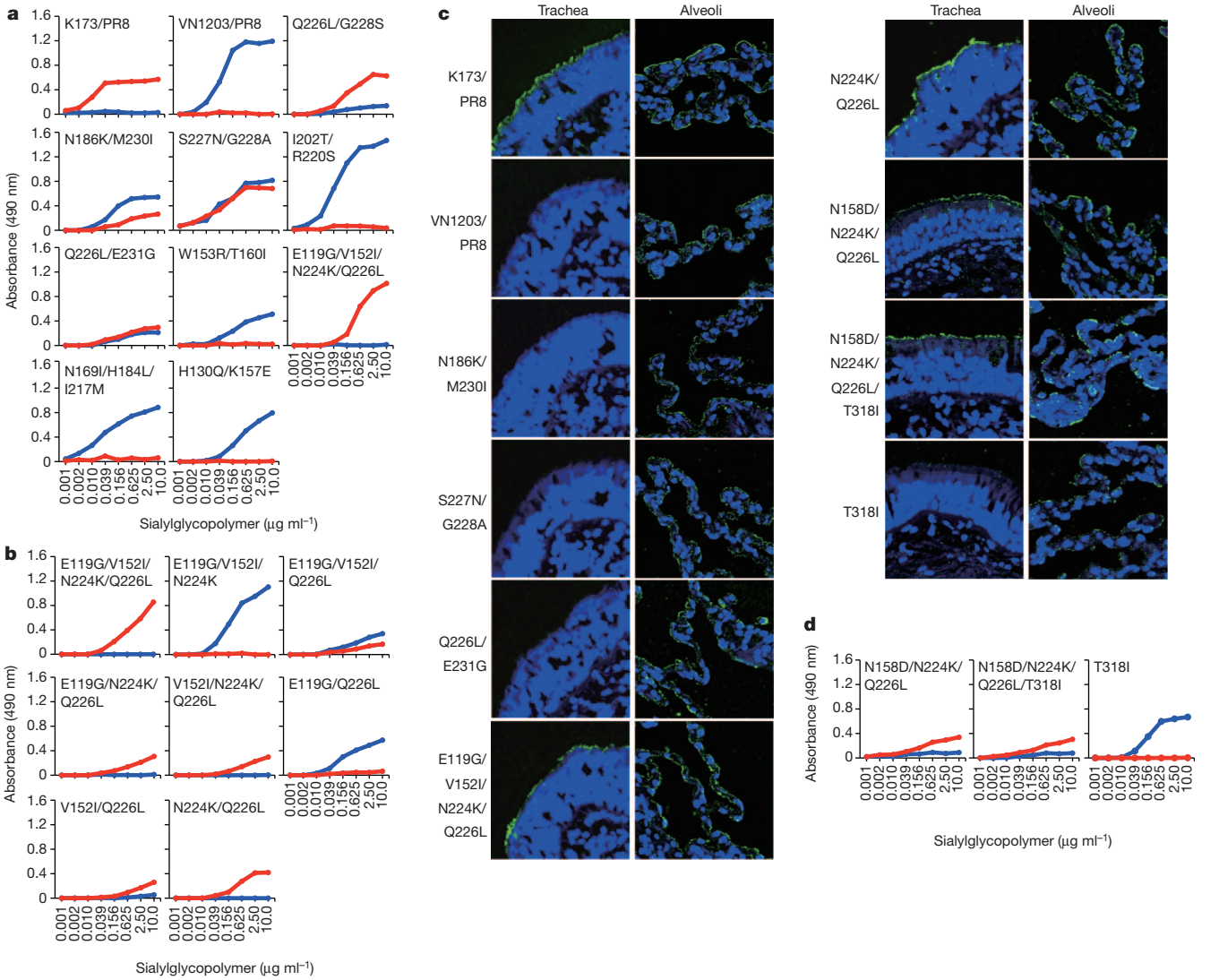

Figure 2 | Characterization of the receptor-binding properties of isolated viruses. **a**, Binding of VN1203 mutants to sialylglycopolymers in solid-phase binding assays. A human virus (K173/PR8), an avian virus (VN1203/PR8) and mutant VN1203/PR8 viruses were compared for their ability to bind to sialylglycopolymers containing either α2,3-linked (blue) or α2,6-linked (red) sialic acids. **b**, Identification of mutations that confer binding to human-type receptors. **c**, Binding of VN1203 mutant viruses to human respiratory tissues. K173/PR8, VN1203/PR8 and mutant VN1203/PR8 viruses were incubated with human tissue sections and then stained with either anti-K173 antiserum (green) or anti-VN1203 HA antibodies (green). All sections were subsequently incubated with labelled secondary antibodies and Hoechst dye (blue). **d**, Characterization of the receptor-binding properties of N158D/N224K/Q226L, N158D/N224K/Q226L/T318I and T318I viruses. The direct binding of virus to sialylglycopolymers containing either α2,3-linked (blue) or α2,6-linked (red) sialic acids was determined as described in panel **a**.

To assess the effect of enhanced α2,6-glycan recognition on the attachment of viruses to human respiratory tracts, sections of tracheal and lung tissues were exposed to K173/PR8 (human-type receptor binder), VN1203/PR8 (avian-type receptor binder) and mutant VN1203/PR8 viruses (Fig. 2c). Because the N186K/M230I, S227N/G228A, Q226L/E231G, E119G/V152I/N224K/Q226L and N224K/Q226L mutants exhibited appreciable binding to Siaα2,6Gal (Fig. 2a, b), the attachment of these mutants was also tested. On tracheal sections, the K173/PR8 virus bound extensively to ciliated epithelial cells (Fig. 2c and Supplementary Fig. 3), whereas the VN1203/PR8 virus bound poorly. By contrast, on lung sections, both viruses bound extensively to the alveolar epithelial surface (both type I and II pneumocytes; Fig. 2c and Supplementary Fig. 4). The binding patterns of these viruses correlate with the distribution of Siaα2,3Gal (that is, avian-type receptors; present in lung epithelia) and Siaα2,6Gal (that is, human-type receptors; present in both trachea and lung epithelia) on the tissues, as observed with lectin staining[18] (Supplementary Fig. 5). Like the human K173/PR8 virus, the E119G/V152I/N224K/Q226L and N224K/Q226L mutants exhibited strong binding to the ciliated epithelial cells of the trachea (Fig. 2c and Supplementary Fig. 3). By contrast, the N186K/M230I, S227N/G228A and Q226L/E231G mutants displayed little-to-no binding to tracheal epithelia (Fig. 2c), despite their binding to Siaα2,6Gal (Fig. 2a). A number of sialylated oligosaccharides with differing branching patterns and chain lengths are thought to be present on the cell surface[19]. We therefore speculate that the mutants can recognize a short glycan structure such as Siaα2,6Galβ1,4GlcNAc, but may not recognize longer, more complex glycan structures, which are possibly required for binding to human tracheal epithelium. On the other hand, all mutants bound to alveolar epithelial cells (both type I and II pneumocytes; Fig. 2c and Supplementary Fig. 4). When the tissue sections were pre-treated with *Arthrobacter ureafaciens* sialidase (which cleaves all non-reducing terminally branched and unbranched sialic acids), virus binding to the tissues was substantially reduced (Supplementary Fig. 6a–c), confirming the sialic acid binding specificity of the virus. These data indicate that alterations in the receptor specificity of the E119G/V152I/N224K/Q226L and N224K/Q226L

mutants have profound effects on virus attachment to human respiratory epithelium.

In an avian H3 HA, the Q226L mutation changed the binding preference from avian- to human-type[20]. A previous study found that the Q226L mutation on an H5 HA does not confer efficient binding to α2,6-glycans in a glycan array[15]; however, when tested in combination with G228S, increased binding to human-type receptors, but not a complete switch from avian- to human-type receptor-binding specificity, was observed[15]. By contrast, here we found that Q226L in combination with N224K resulted in a switch from Siaα2,3Gal to Siaα2,6Gal binding in an H5 HA and allowed virus binding to human tracheal epithelia (Fig. 2c). The receptor-binding domain of HA is formed by the 190-helix at the top of HA, the 220-loop at the edge of the globular head, and the 130-loop at the other edge of the globular head (Fig. 1a). Crystal structure analysis revealed that the 220-loop of avian H5 HA is closer to the opposing 130-loop than in human H3 HA, indicating that a wider binding site for human H3 HA, compared to that of avian H5 HA, may be required to optimize contacts with the larger Siaα2,6-glycans[21]. N224 lies on the turn leading into the 220-loop, adjacent to position 226 (Fig. 1a). Replacement of N224 may alter the orientation of the 220-loop and thus optimize contacts between L226 and Siaα2,6Gal-containing receptors, thereby increasing the preference for α2,6 linkages.

Recent studies reported that 2009 pandemic H1N1 and H5N1 viruses show high genetic compatibility[22,23]. These two viruses have been isolated from pigs[24–28], which have been considered as 'mixing vessels' for the reassortment of avian, swine and human strains. Thus, the coexistence of H5N1 and 2009 pandemic H1N1 viruses could provide an opportunity for the generation of transmissible H5 avian–human reassortants in mammals. Therefore, we generated reassortant viruses possessing the mutant VN1203 HAs generated above, and the seven remaining gene segments from a prototype 2009 pandemic H1N1 virus (A/California/04/2009, CA04). Experiments with viruses possessing the wild-type HA cleavage site were performed in enhanced biosafety level 3 (BSL3+) containment laboratories approved for such use by the Centers for Disease Control and Prevention (CDC) and the United States Department of Agriculture (USDA). Because efficient human-to-human transmission is a critical feature of pandemic influenza viruses, we examined the growth and transmissibility of reassortant viruses in ferrets, which are widely accepted as an animal model for influenza virus transmissibility and pathogenesis studies. Because the E119G/V152I/N224K/Q226L and N224K/Q226L variants bound extensively to human tracheal epithelia (Fig. 2c), we generated by reverse genetics (rg) three H5 reassortant viruses possessing the VN1203 HA or mutant HAs (all with the wild-type multibasic cleavage site) and the remaining genes from the CA04 virus. The VN1203 HA mutants tested included the one containing four mutations, E119G, V152I, N224K and Q226L (designated rg(E119G/V152I/N224K/Q226L)/CA04), and another containing two mutations, N224K and Q226L (designated rg(N224K/Q226L)/CA04).

To determine whether the introduced HA mutations affected the replication of the H5 reassortant viruses, six ferrets were inoculated intranasally with 10^6 plaque-forming units (p.f.u.) of virus. On day 3 after infection, a recombinant virus whose genes all came from CA04, rgCA04, replicated efficiently in the respiratory organs of infected animals, and was isolated from the colon, but not from any other organs tested (Fig. 3 and Supplementary Table 2). A virus possessing H5 VN1203 HA and the remaining genes from CA04 (designated rgVN1203/CA04) replicated to titres comparable to those of rgCA04 in nasal turbinates, but substantially less in the lungs. By contrast, the two H5 reassortant viruses with HA mutations (rg(E119G/V152I/N224K/Q226L)/CA04 and rg(N224K/Q226L)/CA04) were severely limited in their replicative ability in trachea. Although virus titres in nasal turbinates and lung were not statistically different between rg(N224K/Q226L)/CA04 and rgCA04, the virus titre in nasal turbinates was significantly lower in animals inoculated with rg(E119G/V152I/N224K/Q226L)/CA04 than in animals inoculated with rgCA04 (Dunnett's test; $P = 0.0002$; Fig. 3). Notably, rgVN1203/CA04 (avian-type receptor binder) replicated efficiently in nasal turbinates of ferrets, which have a similar sialic acid receptor distribution pattern to that of the human respiratory tract[29,30]. The reason for this discrepancy is unclear; however, replication of avian H5N1 viruses in ferret nasal turbinates has been reported[12,13].

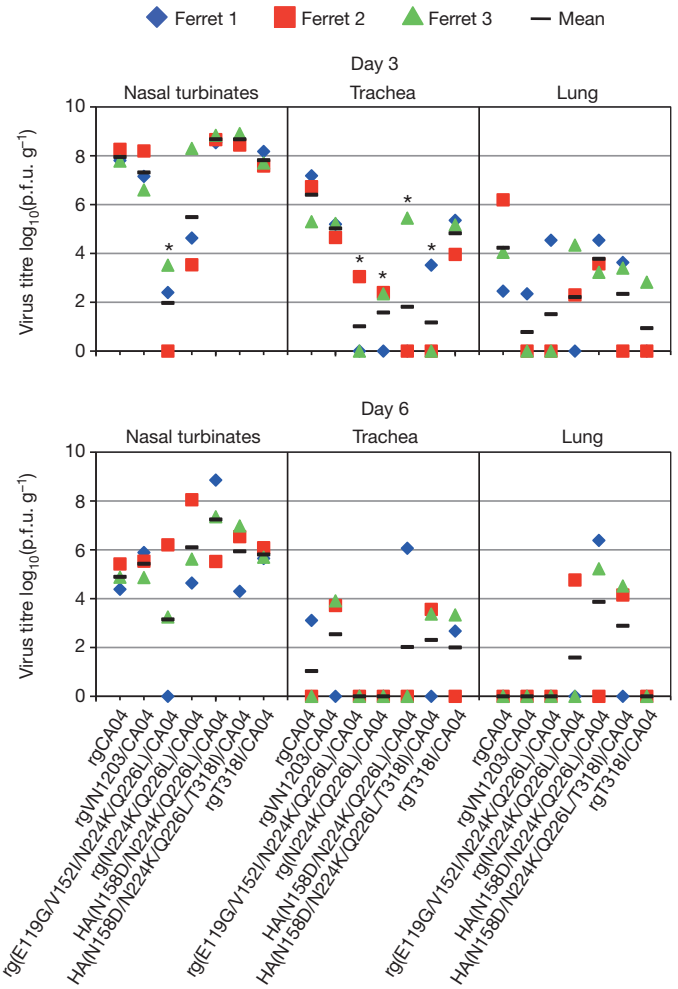

Figure 3 | Virus replication in respiratory organs. Ferrets were infected intranasally with 10^6 p.f.u. of virus. Three ferrets per group were killed on days 3 and 6 after infection for virus titration. Virus titres in nasal turbinates, trachea and lung were determined by use of a plaque assay on MDCK cells. Horizontal bars show the mean. Asterisks indicate virus titres significantly different from that of rgCA04 (Dunnett's test; $P < 0.05$).

Although virus titres in respiratory organs were generally lower on day 6 after infection than on day 3 after infection, rg(N224K/Q226L)/CA04 still showed high levels of replication at day 6 after infection; titres in nasal turbinates ranged from $10^{4.6}$ to $10^{8.1}$ p.f.u. g^{-1} (Fig. 3). Sequence analysis of viruses in nasal turbinates on day 6 after infection revealed that viruses in ferret 2 and ferret 3 possessed N158D and N158K mutations in their HA (in addition to the original two mutations), respectively, leading to the loss of the glycosylation site at position 158 (that is, 158N-S-T to 158D-S-T or 158K-S-T; Fig. 1a and Supplementary Table 3). In nasal turbinates on day 6 after infection, the titre of the virus with the N158D/N224K/Q226L mutations ($10^{8.1}$ p.f.u. g^{-1}; see Fig. 3, ferret 2 of rg(N224K/Q226L)/CA04) was approximately four orders of magnitude higher than that of the original rg(N224K/Q226L)/CA04 ($10^{4.6}$ p.f.u. g^{-1}; Fig. 3, ferret 1 of rg(N224K/Q226L)/CA04), whereas the virus with the N158K/N224K/Q226L mutations ($10^{5.6}$ p.f.u. g^{-1}; Fig. 3, ferret 3 of rg(N224K/Q226L)/CA04) grew to one order of magnitude higher than

the original mutant. These data indicate that the additional mutation N158D improved the replication of rg(N224K/Q226L)/CA04 in ferrets. To test the effect of this mutation on the replication of H5 reassortant viruses in ferrets, we examined the replicative ability of a virus with the triple N158D/N224K/Q226L HA substitutions in ferrets. This HA(N158D/N224K/Q226L)/CA04 virus replicated efficiently in infected animals, except in the trachea (Fig. 3 and Supplementary Table 2). On day 3 after infection, this virus was isolated from the brain of two of the three animals tested, although we did not observe neurological signs in these animals. These results indicate that the N158D mutation contributed to the efficient growth in the nasal turbinates of ferrets of an H5 reassortant virus with the N224K/Q226L mutations. Removal of the glycosylation site at position 158 has been reported to result in enhanced binding of H5N1 viruses to human-type receptors in combination with the Q226L/G228S mutations[7]. A previous study showed that H5N1 viruses lacking this glycosylation site transmit efficiently by direct contact among guinea-pigs[31]. By contrast, H5N1 viruses that acquire this glycosylation site lose the ability to transmit among guinea-pigs. Therefore, we speculated that the loss of the glycosylation site in HA(N158D/N224K/Q226L)/CA04 virus may affect its transmissibility in ferrets.

To assess the ability of H5 reassortant viruses with human-type receptor specificity to transmit between ferrets, we placed naive ferrets in wireframe cages next to ferrets inoculated with 10^6 p.f.u. of rgCA04, rgVN1203/CA04, rg(N224K/Q226L)/CA04, or HA(N158D/N224K/Q226L)/CA04 (Supplementary Fig. 7). Similar to previous experiments[32], rgCA04 was efficiently transmitted via respiratory droplets to all three contact ferrets, as evidenced by the detection of virus in nasal washes and haemagglutination inhibition (HI) antibody in these animals (Table 1 and Fig. 4). By contrast, rgVN1203/CA04 and rg(N224K/Q226L)/CA04 were not transmitted; neither virus shedding nor seroconversion was detected in any contact animals, despite the binding of the latter to Siaα2,6Gal. This result was consistent with that of previous studies in which human-type receptor recognition was shown to be necessary but not sufficient for respiratory droplet transmission of an H5N1 virus in a ferret model[12,14]. In the HA(N158D/N224K/Q226L)/CA04-inoculated group, virus was recovered from two of the six contact ferrets (pairs 1 and 2) between days 5 and 7 after contact. Moreover, seroconversion was detected in five animals including those from which virus was recovered. No animals died in the course of these transmission experiments. This finding demonstrates the generation of an H5 HA that supports virus transmission by respiratory droplets among ferrets.

To determine whether additional mutations occurred in the HA of HA(N158D/N224K/Q226L)/CA04 during transmission, viral RNA was analysed from nasal washes of inoculated and contact ferrets (Fig. 4 and Supplementary Table 4). On day 5 after infection, the A242S and T318I mutations in HA were present in five (pairs 1, 3, 4, 5 and 6) and one (pair 2) of the six inoculated animals, respectively. Viruses derived from the contact animals of pair 1 on day 7 after contact had two changes in HA (K193N and A242S) (Fig. 1a), whereas those derived from the contact animals of pair 2 contained a single change in HA (T318I) (Fig. 1b), indicating that additional changes in HA occurred during the infection of ferrets with HA(N158D/N224K/Q226L)/CA04. No mutations in the remaining genes were detected in any of these viruses from nasal washes compared with the CA04 virus sequences.

Because HA(N158D/N224K/Q226L)/CA04 was isolated from only one-third of the contact animals, we isolated a virus from the nasal wash of the contact ferret that shed a high titre ($10^{7.5}$ p.f.u. ml^{-1}) of virus on day 7 after contact (pair 2) (Fig. 4d) to evaluate the replication and transmissibility of that virus in ferrets. This mutant virus, designated HA(N158D/N224K/Q226L/T318I)/CA04, replicated efficiently in the nasal turbinates and was isolated from brain tissue (Fig. 3 and Supplementary Table 2). In the transmission study, four of the six contact ferrets were positive for virus between days 3 and 7 after contact, and all contact animals were seropositive; no animals died in the course of the transmission experiments (Table 1; Fig. 4e and Supplementary Fig. 8). Notably, this transmission pattern is comparable to that of the 1918 pandemic H1N1 virus when tested under the same experimental conditions; the 1918 pandemic virus was recovered from the nasal wash of two of three contact animals (our own unpublished data). Sequence comparison of viruses from inoculated and contact animals identified mutations at positions 225 and 242 as well as a reversion at position 224 (Fig. 1a and Supplementary Table 5) (in addition to the original four mutations) although the 224 reversion was found only in viruses from inoculated ferrets. Collectively, these findings demonstrate that four amino acid substitutions (N158D/N224K/Q226L/T318I) in H5 HA confer efficient respiratory droplet transmission in ferrets to a virus possessing an H5 HA in a 2009 pandemic H1N1 backbone. We also confirmed that recombinant viruses possessing the three HA mutations N158D, N224K and Q226L, or the four HA mutations N158D, N224K, Q226L and T318I, and the NA of VN1203 in a PR8 backgrand (designated N158D/N224K/Q226L or N158D/N224K/Q226L/T318I, respectively) preferentially bind to Siaα2,6Gal and attach to human tracheal epithelia (Fig. 2c, d).

HA(N158D/N224K/Q226L/T318I)/CA04 transmitted by respiratory droplet more efficiently than HA(N158D/N224K/Q226L)/CA04, raising the possibility that the T318I mutation is involved in the efficient transmission of avian H5N1/pandemic H1N1 reassortants. To explore the functional role of this mutation in respiratory droplet transmission, we generated an H5 reassortant expressing the H5 HA with the T318I mutation and examined its receptor-binding specificity and transmissibility. This reassortant (designated rgT318I/CA04) bound to only Siaα2,3Gal and showed little binding to human tracheal epithelia (Fig. 2c, d). rgT318I/CA04 did not transmit via respiratory droplet among ferrets (Table 1 and Fig. 4f), although it replicated in nasal turbinates and trachea as efficiently as rgCA04 (Fig. 3 and Supplementary Table 2). These results indicate that the T318I mutation alone is not sufficient for H5 reassortant viruses to transmit efficiently among ferrets.

Table 1 | Transmission in ferrets inoculated with H5 avian–human reassortant viruses

Virus	Inoculated ferrets			Contact ferrets	
	Weight loss (%)*	Peak virus titre in nasal wash (mean $\log_{10}$(p.f.u. ml^{-1})) (days after inoculation)	Seroconversion (positive and total numbers) (HI titre)†	Virus detection in nasal wash (positive and total numbers)	Seroconversion (positive and total numbers) (HI titre)
rgCA04	3 of 3 (15.1)	7.5 (1)	3 of 3 (≥1,280, ≥1,280, ≥1,280)	3 of 3	3 of 3 (≥1,280, ≥1,280, ≥1,280)
rgVN1203/CA04	3 of 3 (5.9)	5.3 (5)	3 of 3 (80, 40, 80)	0 of 3	0 of 3 (<10, <10, <10)
rg(N224K/Q226L)/CA04	2 of 3 (7.8)‡	3.9 (5)	3 of 3 (≥1,280, ≥1,280, ≥1,280)	0 of 3	0 of 3 (<10, <10, <10)
HA(N158D/N224K/Q226L)/CA04	6 of 6 (5.7)	6.7 (3)	6 of 6 (640, ≥1,280, ≥1,280, 640, ≥1,280, ≥1,280)	2 of 6	5 of 6 (160, 320, 20, 160, 40, <10)
HA(N158D/N224K/Q226L/T318I)/CA04	6 of 6 (9.8)	6.1 (5)	6 of 6 (≥1,280, ≥1,280, 640, ≥1,280, ≥1,280, ≥1,280)	4 of 6	6 of 6 (640, 640, ≥1280, 80, ≥1,280, 320)
rgT318I/CA04	3 of 5 (1.5)§	5.6 (3)	5 of 5 (40, 20, 20, 40, 40)	0 of 5	0 of 5 (<10, <10, <10, <10, <10)

* Maximum percentage weight loss is shown.
† Haemagglutination inhibition (HI) assays were carried out with homologous virus and turkey red blood cells.
‡ One animal did not lose any body weight.
§ Two animals did not lose any body weight.

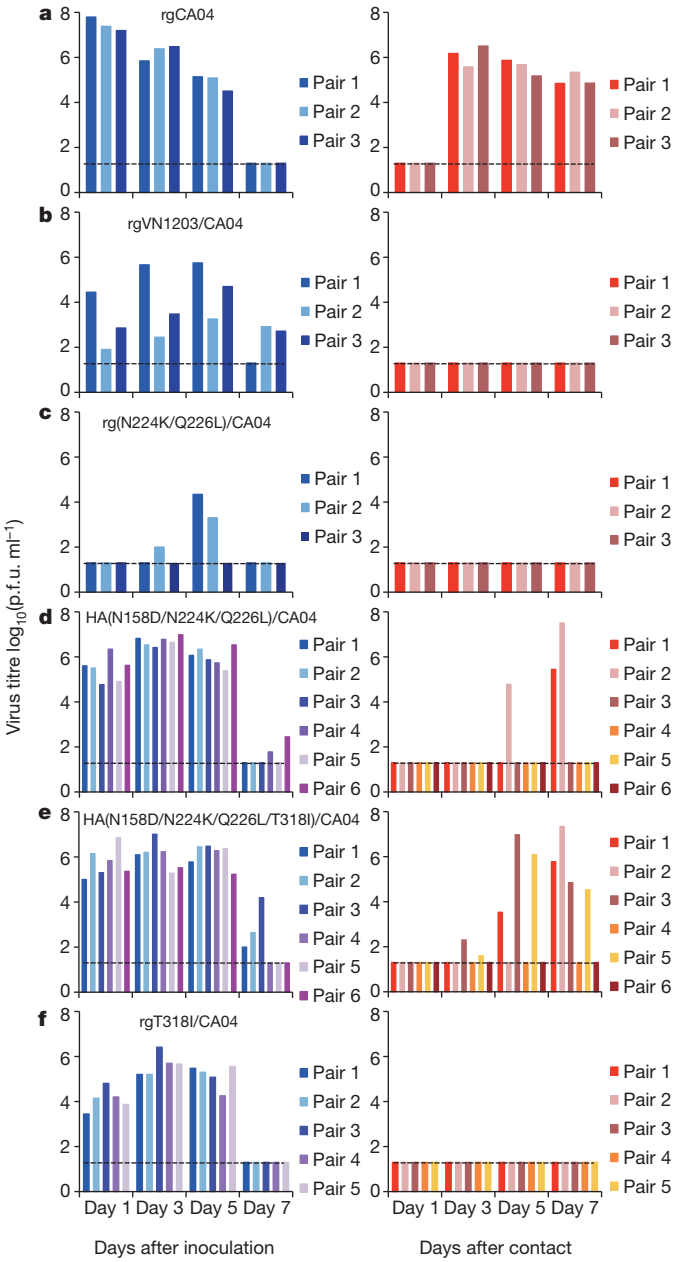

Figure 4 | Respiratory droplet transmission of H5 avian–human reassortant viruses in ferrets. a–f, Groups of three, five, or six ferrets were inoculated intranasally with 10^6 p.f.u. of rgCA04 (**a**), rgVN1203/CA04 (**b**), rg(N224K/Q226L)/CA04 (**c**), HA(N158D/N224K/Q226L)/CA04 (**d**), HA(N158D/N224K/Q226L/T318I)/CA04 (**e**), or rgT318I/CA04 (**f**). One day after infection, three, five, or six naive ferrets were placed in adjacent cages. Nasal washes were collected every other day from both inoculated (left panel) and contact (right panel) animals for virus titration. Virus titres in organs were determined by using a plaque assay on MDCK cells. The lower limit of detection is indicated by the horizontal dashed line.

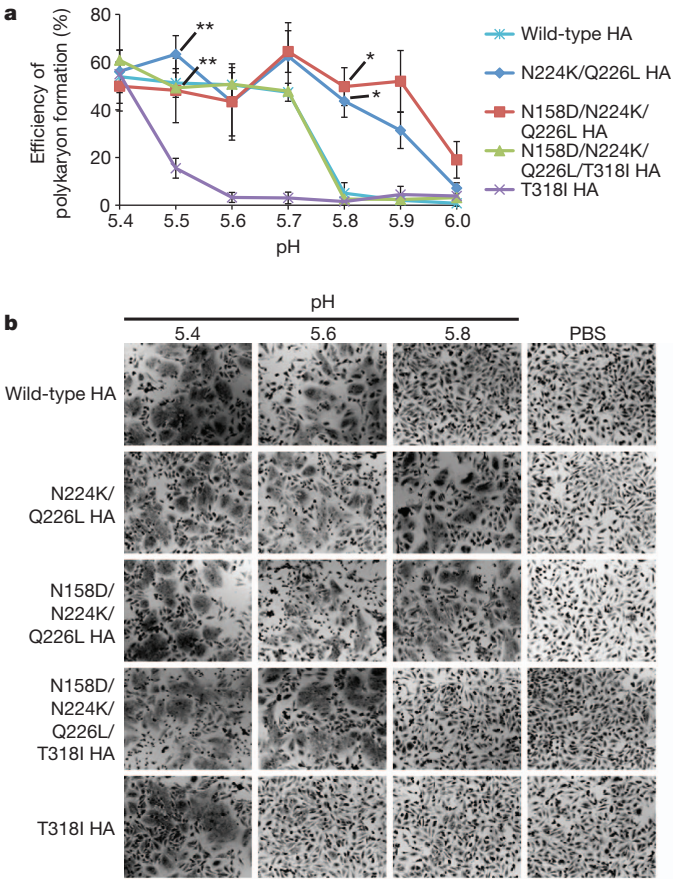

Figure 5 | Polykaryon formation by HeLa cells expressing wild-type or mutant HAs after acidification at low pH. a, The efficiency of polykaryon formation over a pH range of 5.4–6.0 was estimated from the number of nuclei in polykaryons divided by the total number of nuclei in the same field. The mean and standard deviations determined from five randomly chosen fields of cell culture are shown. Single asterisks indicate values significantly different between the wild-type HA and the N224K/Q226L or N158D/N224K/Q226L HA (Tukey test; $P < 0.05$). The double asterisk indicates values significantly different between the T318I HA and the N224K/Q226L or N158D/N224K/Q226L HA (Tukey test; $P < 0.05$). **b**, Representative fields of cells expressing the indicated HAs and exposed to pH 5.4, 5.6, or 5.8 are shown. Images were taken at ×10 magnification.

Influenza virus HA protein has membrane-fusion as well as receptor-binding activity. Notably, in the three-dimensional model of influenza A virus HA, residue 318 is located proximally to the fusion peptide (Fig. 1b), which has key roles in the membrane fusion process. To assess the effect of HA mutations on low-pH-induced membrane fusion activity, we examined the pH at which the fusion activity of wild-type and mutant HA was activated (Fig. 5). The wild-type HA had a threshold for membrane fusion of pH 5.7; the N224K/Q226L and N158D/N224K/Q226L mutations raised the threshold for fusion to >pH 5.9, whereas the T318I mutation reduced the threshold for fusion to pH 5.5. The N158D/N224K/Q226L/T318I mutations showed wild-type fusogenic properties (that is, a threshold at pH 5.7). The HA of influenza virus undergoes a low-pH-dependent conformational change, which is required for fusion of the viral envelope with the target membrane[33]. Such a conformational change to a fusion-active form can also lead to viral inactivation. Therefore, sustained and efficient human-to-human transmission of virus may require a certain level of stability of the HA protein in an acidic environment, as the pH of human nasal mucosa, where human influenza viruses replicate primarily, is approximately pH 5.5–6.5 (ref. 34). Our findings suggest that an increase in the pH threshold for fusion as a result of the N224K/Q226L mutations that shift the HA receptor recognition from avian-type to human-type may reduce HA protein stability; however, the T318I mutation decreases the pH threshold for fusion activity, resulting in a stable mutant HA.

Because heat treatment at neutral pH is also known to promote a fusogenic form of HA protein[35,36] and serve as a surrogate assay for HA stability[37], we next tested whether the HA mutations described above affect the heat stability of the HA protein. Wild-type and mutant HA viruses were incubated at 50 °C for various times, after which the loss of infectivity and haemagglutination activity were determined. The wild-type and N224K/Q226L viruses lost most of their infectivity by heating for 60 min (>5.5-$\log_{10}$ decrease in titre; Fig. 6a), whereas the

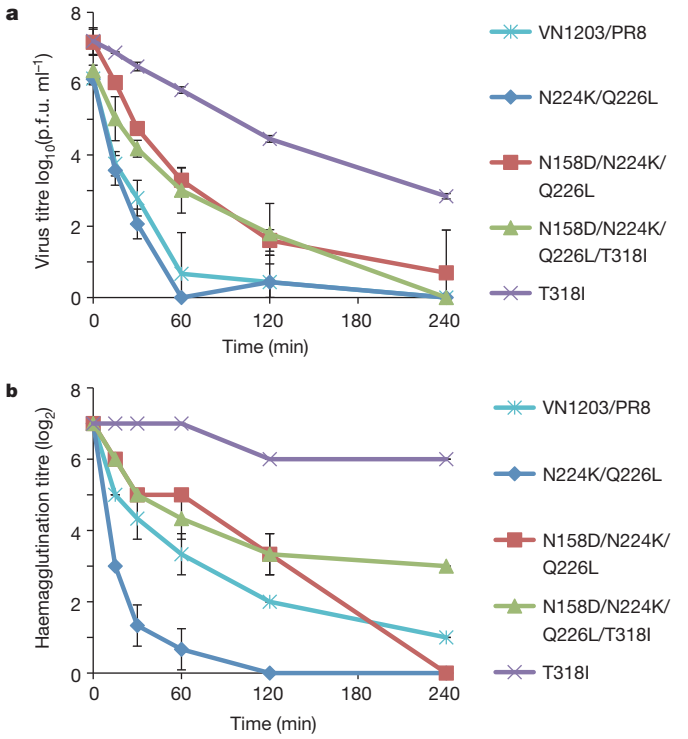

Figure 6 | Effect of heat treatment on the infectivity and haemagglutination activity of viruses. Aliquots of a virus stock containing 128 HA units were incubated for the times indicated at 50 °C. **a**, Virus titres in heat-treated samples were determined by plaque assays on MDCK cells. **b**, Haemagglutination titres in heat-treated samples were determined by using haemagglutination assays with 0.5% TRBCs. Each point represents the mean ± standard deviation from triplicate experiments.

N158D/N224K/Q226L and N158D/N224K/Q226L/T318I mutants exhibited considerable tolerance to high temperature (3.9- and 3.4-$\log_{10}$ decrease after a 60-min incubation, respectively) and the T318I mutant was most resistant (only a 1.4-$\log_{10}$ decrease under the same conditions). In haemagglutination assays, the N224K/Q226L mutant HA lost activity more rapidly than did the wild-type HA, and N158D/N224K/Q226L lost activity more rapidly than did the N158D/N224K/Q226L/T318I mutant (Fig. 6b). Thus, addition of the N158D mutation to the N224K/Q226L HA increased HA stability and subsequent addition of the fourth mutation, T318I, rendered the HA protein even more stable. Taken together, these results suggest that the addition of the T318I mutation to H5 HAs that preferentially recognize human-type receptors restores HA protein stability, thereby allowing a virus carrying the N158D/N224K/Q226L/T318I mutations in HA to transmit efficiently via respiratory droplet among ferrets. In conclusion, a fine balance of mutations affecting different functions in HA (such as receptor-binding specificity and HA stability) may be critical to confer transmissibility in ferrets.

We next compared the pathogenicity in ferrets of H5 avian–human reassortants with that of the pandemic H1N1 virus CA04 (Fig. 7, Supplementary Information and Supplementary Figs 9–11). The control virus, rgCA04, caused substantial body weight loss (15.1%) (Table 1 and Supplementary Fig. 9). By contrast, the four reassortant viruses caused only modest weight loss (<10%) in most of the animals. However, no statistically significant differences in body weight loss were found between the reassortant viruses and rgCA04. Pathological examination revealed similar histological changes and levels of viral antigens in the nasal mucosa of rgCA04-, HA(N158D/N224K/Q226L)/CA04- and HA(N158D/N224K/Q226L/T318I)/CA04-infected ferrets (Fig. 7a, b). In the rgVN1203/CA04 and rg(N224K/Q226L)/CA04 groups, however, less tissue damage was found in the nasal mucosa compared with the rgCA04 group on day 3 after infection (Dunnett's test; $P = 0.0057$ and 0.0175, respectively; Fig. 7b). In addition, all three

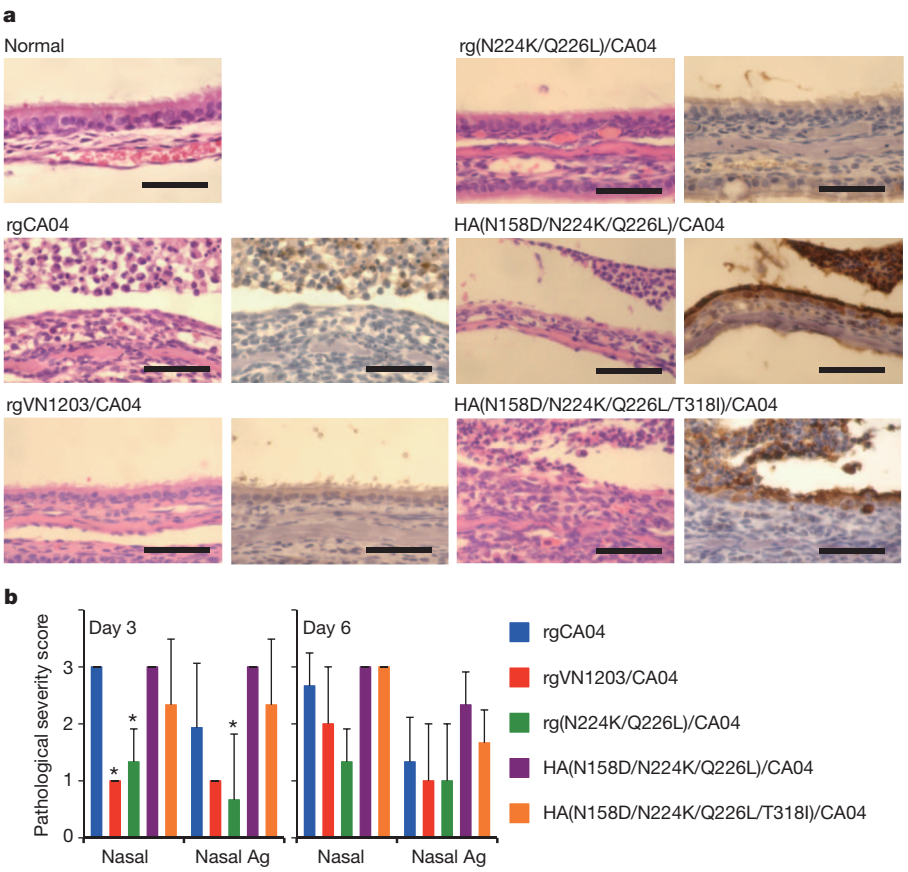

Figure 7 | Pathological analyses of H5 avian–human reassortant viruses. **a**, Representative histological changes in nasal turbinates from influenza-virus-infected ferrets. Three ferrets per group were infected intranasally with 10^6 p.f.u. of virus, and tissues were collected on day 3 after infection for pathological examination. Uninfected ferret tissues served as negative controls (normal). Left panel, haematoxylin-and-eosin staining. Right panel, immunohistochemical staining for viral antigen detection (brown staining). Scale bars, 50 μm. **b**, Pathological severity scores in infected ferrets. To represent comprehensive histological changes, respiratory tissue slides were evaluated by scoring the pathological changes and viral antigen expression levels. The pathological scores were determined for each animal in each group ($n = 3$ per group on days 3 and 6 after infection) using the following scoring system: 0, no pathological change/antigen negative; 1, affected area (<30%) or only interstitial lesion/rare viral antigens; 2, affected area (<80%, ≥30%)/moderate viral antigens; 3, severe lesion (≥80%)/many viral antigens. Nasal, pathological changes in the nasal mucosa; nasal Ag, viral antigens in the nasal mucosa. Asterisks indicate virus pathological scores significantly different from that of rgCA04 (Dunnett's test; $P < 0.05$). Error bars denote standard deviation.

viruses caused lung lesions (Supplementary Information and Supplementary Figs 10 and 11).

To assess whether current control measures may be effective against the H5 transmissible reassortant mutant virus, we examined the reactivity of sera from individuals vaccinated with an H5N1 prototype vaccine[38] against a virus possessing the N158D/N224K/Q226L/T318I mutations in HA. We found that pooled human sera from individuals immunized with this vaccine reacted with the virus possessing the mutant H5 HA (N158D/N224K/Q226L/T318I) at a higher titre than with a wild-type H5 HA virus (VN1203/PR8; Supplementary Table 6), indicating that current H5N1 vaccines would be efficacious against the H5 transmissible reassortant mutant virus. In addition, the H5 transmissible reassortant mutant virus (HA(N158D/N224K/Q226L/T318I)/CA04) was highly susceptible to a licensed NA inhibitor, oseltamivir (Supplementary Table 7). These experiments show that appropriate control measures would be available to combat the transmissible virus described in this study.

Currently, we do not know whether the mutations that we identified in this study that allowed the HA(N158D/N224K/Q226L/T318I)/CA04 virus to be transmissible in ferrets would also support sustained human-to-human transmission. In particular, we wish to emphasize that the transmissible HA(N158D/N224K/Q226L/T318I)/CA04 virus possesses seven segments (all but the HA segment) from a human pandemic 2009 H1N1 virus. Human-virus-characteristic amino acids in these seven segments may have critically contributed to the respiratory droplet transmission of the HA(N158D/N224K/Q226L/T318I)/CA04 virus in ferrets. Examples include amino acids in the PB2 polymerase protein that confer efficient replication in mammalian, but not avian, cells[39–43]. As the PB2 gene of the HA(N158D/N224K/Q226L/T318I)/CA04 virus is of human virus origin, the virus possesses high replicative ability in mammalian cells. In contrast, most avian virus PB2 proteins lack these human-type amino acids, although one of these changes (a glutamic-acid-to-lysine mutation at position 627) is found in highly pathogenic avian H5N1 viruses circulating in the Middle East[44]. As a second example, the viral NA gene may contribute to viral transmissibility. The NA protein cleaves α-ketosidic linkages between a terminal sialic acid and an adjacent sugar residue, an activity that balances the sialic-acid-binding activity of HA. A recent study found that a human virus NA gene was critical to confer limited transmissibility to a mutant H5 avian-human reassortant virus[14]. In general, a human-type receptor recognizing H5 HA alone may not be sufficient to confer transmissibility in mammals, but may have to act together with other human-virus-characteristic traits (in PB2, NA, and/or other viral proteins). Therefore, at this point we cannot predict whether the four mutations in the H5 HA identified here would render a wholly avian H5N1 virus transmissible.

Three of the residues identified here (N224, Q226 and T318) have been strictly conserved among H5 HA proteins isolated since 2003. However, as H5N1 viruses continue to evolve and infect people, receptor-binding variants of H5N1 viruses, including avian–human reassortant viruses as tested here, may emerge. One of the four mutations we identified in our transmissible virus, the N158D mutation, results in loss of a glycosylation site. Many H5N1 viruses isolated in the Middle East, Africa, Asia and Europe do not have this glycosylation site. Therefore, only three nucleotide changes are needed for the HA of these viruses to support efficient transmission in ferrets. In addition, the H5N1 viruses circulating in these geographic areas also possess a glutamic-acid-to-lysine mutation at position 627 in the PB2 protein, which promotes viral replication in certain mammals, including humans[40,45]. Therefore, these viruses may be several steps closer to those capable of efficient transmission in humans and are of concern.

Our study highlights the pandemic potential of viruses possessing an H5 HA. Although current vaccines may protect against a virus similar to that tested here, the continued evolution of H5N1 viruses reinforces the need to prepare and update candidate vaccines to H5 viruses. The amino acid changes identified here will help individuals conducting surveillance in regions with circulating H5N1 viruses (for example, Egypt, Indonesia, Vietnam) to recognize key residues that predict the pandemic potential of isolates. Rapid responses in a potential pandemic situation are essential in order to generate appropriate vaccines and initiate other public health measures to control infection. Furthermore, our findings are of critical importance to those making public health and policy decisions.

Our research answers a fundamental question in influenza research: can H5-HA-possessing viruses support transmission in mammals? Moreover, our findings have suggested that different mechanisms (that is, receptor-binding specificity and HA stability) may act in concert for efficient transmissibility in mammals. This knowledge will facilitate the identification of additional mutations that affect viral transmissibility; the monitoring of this expanded set of changes in natural isolates may improve our ability to assess the pandemic potential of H5N1 viruses. Thus, although a pandemic H5N1 virus may not possess the amino acid changes identified in our study, the findings described here will advance our understanding of the mechanisms and evolutionary pathways that contribute to avian influenza virus transmission in mammals.

METHODS SUMMARY

Viruses. All recombinant viruses were generated by using reverse genetics essentially as described previously[16]. All experiments with the viruses possessing the wild-type HA cleavage site were performed in an enhanced biosafety level 3 (BSL3+) containment laboratory approved for such use by the CDC and the USDA.

Infection and transmission in ferrets. Six–ten-month-old female ferrets (Triple F Farms) were intramuscularly anaesthetized and intranasally inoculated with 10^6 p.f.u. (500 μl) of virus. On days 3 and 6 after infection, ferrets were killed for virological and pathological examinations. The virus titres in various organs were determined by use of plaque assays in MDCK cells.

For transmission studies in ferrets, animals were housed in adjacent transmission cages that prevented direct and indirect contact between animals but allowed spread of influenza virus through the air (Showa Science; Supplementary Fig. 7). Ferrets were intranasally inoculated with 10^6 p.f.u. (500 μl) of virus (inoculated ferrets). Twenty-four hours after infection, naive ferrets were each placed in a cage adjacent to an inoculated ferret (contact ferrets). To assess viral replication in the nasal turbinates, we determined viral titres in nasal washes collected from virus-inoculated and contact ferrets on day 1 after inoculation or co-housing, respectively, and then every other day. Animal studies were performed in accordance with Animal Care and Use Committee guidelines of the University of Wisconsin-Madison.

Biosafety and biosecurity. All recombinant DNA protocols were approved by the University of Wisconsin-Madison's Institutional Biosafety Committee after risk assessments were conducted by the Office of Biological Safety, and by the University of Tokyo's Subcommittee on Living Modified Organisms, and, when required, by the competent minister of Japan. In addition, the University of Wisconsin-Madison Biosecurity Task Force regularly reviews the research program and ongoing activities of the laboratory. The task force has a diverse skill set and provides support in the areas of biosafety, facilities, compliance, security and health. Members of the Biosecurity Task Force are in frequent contact with the principal investigator and laboratory personnel to provide oversight and assure biosecurity. Experiments with viruses possessing the wild-type HA cleavage site were performed in enhanced BSL3 containment laboratories approved for such use by the CDC and the USDA. Ferret transmission studies were conducted by three scientists with both DVM and PhD degrees who each had more than a minimum of 6 years of experience with highly pathogenic influenza viruses and animal studies with highly pathogenic viruses. Our staff wear powered air-purifying respirators that filter the air, and disposable coveralls; they shower out on exit from the facility. The containment facilities at University of Wisconsin-Madison were designed to exceed standards outlined in Biosafety in Microbiological and Biomedical Laboratories (5th edition; http://www.cdc.gov/biosafety/publications/bmbl5/BMBL.pdf). Features of the BSL3-enhanced suites include entry/exit through a shower change room, effluent decontamination, negative air-pressure laboratories, double-door autoclaves, double HEPA-filtered exhaust air, and gas decontamination ports. The BSL3-Agriculture suite features include all those listed for BSL3-enhanced plus HEPA-filtered supply and double-HEPA-filtered exhaust air, double-gasketed watertight and airtight seals, airtight dampers on all ductwork, and the structure was pressure-decay tested during commissioning. The University of Wisconsin-Madison facility has a dedicated alarm system that monitors all building controls and sends alarms (~500 possible alerts). Redundancies and emergency resources are built-in to the facility including two

air handlers, two compressors, two filters each place filters are needed, two effluent sterilization tanks, two power feeds to the building, an emergency generator in case of a power failure and other physical containment measures in the facility that operate without power. Biosecurity monitoring of the facility is ongoing. All personnel undergo Select Agent security risk assessment by the United States Criminal Justice Information Services Division and complete rigorous biosafety, BSL3 and Select Agent training before participating in BSL3-level experiments. Refresher training is scheduled on a regular basis. The principal investigator participates in training sessions and emphasizes compliance to maintain safe operations and a responsible research environment. The laboratory occupational health plan is in compliance with the University of Wisconsin-Madison Occupational Health Program. Select agent virus inventory is checked monthly and submitted to the University of Wisconsin-Madison Research Compliance Specialist. Virus inventory is submitted 1–2 times per year to the file holder in the Select Agent branch of the CDC. The research program, procedures, occupational health plan, documentation, security and facilities are reviewed annually by the University of Wisconsin-Madison Responsible Official and at regular intervals by the CDC and the Animal and Plant Health Inspection Service (APHIS) as part of the University of Wisconsin-Madison Select Agent Program.

Full Methods and any associated references are available in the online version of the paper at www.nature.com/nature.

Received 18 August 2011; accepted 9 March 2012.
Published online 2 May 2012.

1. Glaser, L. *et al.* A single amino acid substitution in 1918 influenza virus hemagglutinin changes receptor binding specificity. *J. Virol.* **79,** 11533–11536 (2005).
2. Matrosovich, M. *et al.* Early alterations of the receptor-binding properties of H1, H2, and H3 avian influenza virus hemagglutinins after their introduction into mammals. *J. Virol.* **74,** 8502–8512 (2000).
3. Rogers, G. N. & Paulson, J. C. Receptor determinants of human and animal influenza virus isolates: differences in receptor specificity of the H3 hemagglutinin based on species of origin. *Virology* **127,** 361–373 (1983).
4. Auewarakul, P. *et al.* An avian influenza H5N1 virus that binds to a human-type receptor. *J. Virol.* **81,** 9950–9955 (2007).
5. Gambaryan, A. *et al.* Evolution of the receptor binding phenotype of influenza A (H5) viruses. *Virology* **344,** 432–438 (2006).
6. Stevens, J. *et al.* Recent avian H5N1 viruses exhibit increased propensity for acquiring human receptor specificity. *J. Mol. Biol.* **381,** 1382–1394 (2008).
7. Wang, W. *et al.* Glycosylation at 158N of the hemagglutinin protein and receptor binding specificity synergistically affect the antigenicity and immunogenicity of a live attenuated H5N1 A/Vietnam/1203/2004 vaccine virus in ferrets. *J. Virol.* **84,** 6570–6577 (2010).
8. Watanabe, Y. *et al.* Acquisition of human-type receptor binding specificity by new H5N1 influenza virus sublineages during their emergence in birds in Egypt. *PLoS Pathog.* **7,** e1002068 (2011).
9. Yamada, S. *et al.* Haemagglutinin mutations responsible for the binding of H5N1 influenza A viruses to human-type receptors. *Nature* **444,** 378–382 (2006).
10. Jackson, S. *et al.* Reassortment between avian H5N1 and human H3N2 influenza viruses in ferrets: a public health risk assessment. *J. Virol.* **83,** 8131–8140 (2009).
11. Maines, T. R. *et al.* Lack of transmission of H5N1 avian-human reassortant influenza viruses in a ferret model. *Proc. Natl Acad. Sci. USA* **103,** 12121–12126 (2006).
12. Maines, T. R. *et al.* Effect of receptor binding domain mutations on receptor binding and transmissibility of avian influenza H5N1 viruses. *Virology* **413,** 139–147 (2011).
13. Yen, H. L. *et al.* Inefficient transmission of H5N1 influenza viruses in a ferret contact model. *J. Virol.* **81,** 6890–6898 (2007).
14. Chen, L. M. *et al. In vitro* evolution of H5N1 avian influenza virus toward human-type receptor specificity. *Virology* **422,** 105–113 (2012).
15. Stevens, J. *et al.* Structure and receptor specificity of the hemagglutinin from an H5N1 influenza virus. *Science* **312,** 404–410 (2006).
16. Neumann, G. *et al.* Generation of influenza A viruses entirely from cloned cDNAs. *Proc. Natl Acad. Sci. USA* **96,** 9345–9350 (1999).
17. Hatakeyama, S. *et al.* Enhanced expression of an α2,6-linked sialic acid on MDCK cells improves isolation of human influenza viruses and evaluation of their sensitivity to a neuraminidase inhibitor. *J. Clin. Microbiol.* **43,** 4139–4146 (2005).
18. Shinya, K. *et al.* Avian flu: influenza virus receptors in the human airway. *Nature* **440,** 435–436 (2006).
19. Varki, A. Glycan-based interactions involving vertebrate sialic-acid-recognizing proteins. *Nature* **446,** 1023–1029 (2007).
20. Rogers, G. N. *et al.* Host-mediated selection of influenza virus receptor variants. Sialic acid-α2,6Gal-specific clones of A/duck/Ukraine/1/63 revert to sialic acid-α2,3Gal-specific wild type *in ovo*. *J. Biol. Chem.* **260,** 7362–7367 (1985).
21. Ha, Y., Stevens, D. J., Skehel, J. J. & Wiley, D. C. X-ray structures of H5 avian and H9 swine influenza virus hemagglutinins bound to avian and human receptor analogs. *Proc. Natl Acad. Sci. USA* **98,** 11181–11186 (2001).
22. Cline, T. D. *et al.* Increased pathogenicity of a reassortant 2009 pandemic H1N1 influenza virus containing an H5N1 hemagglutinin. *J. Virol.* **85,** 12262–12270 (2011).
23. Octaviani, C. P., Ozawa, M., Yamada, S., Goto, H. & Kawaoka, Y. High level of genetic compatibility between swine-origin H1N1 and highly pathogenic avian H5N1 influenza viruses. *J. Virol.* **84,** 10918–10922 (2010).
24. Li, H. *et al.* Isolation and characterization of H5N1 and H9N2 influenza viruses from pigs in China [in Chinese]. *Chin. J. Prev. Vet. Med.* **26,** 1–6 (2004).
25. Nidom, C. A. *et al.* Influenza A (H5N1) viruses from pigs, Indonesia. *Emerg. Infect. Dis.* **16,** 1515–1523 (2010).
26. Pasma, T. & Joseph, T. Pandemic (H1N1) 2009 infection in swine herds, Manitoba, Canada. *Emerg. Infect. Dis.* **16,** 706–708 (2010).
27. Pereda, A. *et al.* Pandemic (H1N1) 2009 outbreak on pig farm, Argentina. *Emerg. Infect. Dis.* **16,** 304–307 (2010).
28. Welsh, M. D. *et al.* Initial incursion of pandemic (H1N1) 2009 influenza A virus into European pigs. *Vet. Rec.* **166,** 642–645 (2010).
29. Xu, Q., Wang, W., Cheng, X., Zengel, J. & Jin, H. Influenza H1N1 A/Solomon Island/3/06 virus receptor binding specificity correlates with virus pathogenicity, antigenicity, and immunogenicity in ferrets. *J. Virol.* **84,** 4936–4945 (2010).
30. van Riel, D. *et al.* Human and avian influenza viruses target different cells in the lower respiratory tract of humans and other mammals. *Am. J. Pathol.* **171,** 1215–1223 (2007).
31. Gao, Y. *et al.* Identification of amino acids in HA and PB2 critical for the transmission of H5N1 avian influenza viruses in a mammalian host. *PLoS Pathog.* **5,** e1000709 (2009).
32. Itoh, Y. *et al. In vitro* and *in vivo* characterization of new swine-origin H1N1 influenza viruses. *Nature* **460,** 1021–1025 (2009).
33. Skehel, J. J. & Wiley, D. C. Receptor binding and membrane fusion in virus entry: the influenza hemagglutinin. *Annu. Rev. Biochem.* **69,** 531–569 (2000).
34. England, R. J., Homer, J. J., Knight, L. C. & Ell, S. R. Nasal pH measurement: a reliable and repeatable parameter. *Clin. Otolaryngol. Allied Sci.* **24,** 67–68 (1999).
35. Carr, C. M., Chaudhry, C. & Kim, P. S. Influenza hemagglutinin is spring-loaded by a metastable native conformation. *Proc. Natl Acad. Sci. USA* **94,** 14306–14313 (1997).
36. Haywood, A. M. & Boyer, B. P. Time and temperature dependence of influenza virus membrane fusion at neutral pH. *J. Gen. Virol.* **67,** 2813–2817 (1986).
37. Krenn, B. M. *et al.* Single HA2 mutation increases the infectivity and immunogenicity of a live attenuated H5N1 intranasal influenza vaccine candidate lacking NS1. *PLoS ONE* **6,** e18577 (2011).
38. Treanor, J. J., Campbell, J. D., Zangwill, K. M., Rowe, T. & Wolff, M. Safety and immunogenicity of an inactivated subvirion influenza A (H5N1) vaccine. *N. Engl. J. Med.* **354,** 1343–1351 (2006).
39. Bussey, K. A., Bousse, T. L., Desmet, E. A., Kim, B. & Takimoto, T. PB2 residue 271 plays a key role in enhanced polymerase activity of influenza A viruses in mammalian host cells. *J. Virol.* **84,** 4395–4406 (2010).
40. Hatta, M., Gao, P., Halfmann, P. & Kawaoka, Y. Molecular basis for high virulence of Hong Kong H5N1 influenza A viruses. *Science* **293,** 1840–1842 (2001).
41. Li, Z. *et al.* Molecular basis of replication of duck H5N1 influenza viruses in a mammalian mouse model. *J. Virol.* **79,** 12058–12064 (2005).
42. Mehle, A. & Doudna, J. A. Adaptive strategies of the influenza virus polymerase for replication in humans. *Proc. Natl Acad. Sci. USA* **106,** 21312–21316 (2009).
43. Yamada, S. *et al.* Biological and structural characterization of a host-adapting amino acid in influenza virus. *PLoS Pathog.* **6,** e1001034 (2010).
44. Salzberg, S. L. *et al.* Genome analysis linking recent European and African influenza (H5N1) viruses. *Emerg. Infect. Dis.* **13,** 713–718 (2007).
45. Subbarao, E. K., London, W. & Murphy, B. R. A single amino acid in the PB2 gene of influenza A virus is a determinant of host range. *J. Virol.* **67,** 1761–1764 (1993).

Supplementary Information is linked to the online version of the paper at www.nature.com/nature.

Acknowledgements The authors would like to acknowledge D. Holtzman for his contributions to the initial concept for this project and thoughtful scientific discussions. We thank M. McGregor, R. Moritz, L. Burley, K. Moore, A. Luka, J. Bettridge, N. Fujimoto and M. Ito for technical support, S. Watson for editing the manuscript, and the National Institute of Hygiene and Epidemiology, Hanoi, Vietnam for the A/Vietnam/1203/2004 (H5N1) virus, which was obtained from the CDC. This work was supported by the Bill & Melinda Gates Foundation (Grants 48339 and OPPGH5383), by a Grant-in-Aid for Specially Promoted Research from the Ministry of Education, Culture, Sports, Science, and Technology of Japan, by ERATO (Japan Science and Technology Agency), and by the National Institute of Allergy and Infectious Diseases Public Health Service Research grants. The following reagents were obtained from the NIH Biodefense and Emerging Infections Research Resources Repository, NIAID, NIH: polyclonal anti-monovalent influenza subvirion vaccine rgA/Vietnam/1203/2004 (H5N1), (antiserum, Human), high tire pool, NR-4109 and low titre pool, NR-4110.

Author Contributions M.I., T.W., M.H., S.C.D., M.O., K.S., G.Z., A.H., H.K., S.W., C.L., S.Y., M.K., Y.S., E.A.M., G.N. and Y.K. designed the experiments; M.I., T.W., M.H., S.C.D., M.O., K.S., G.Z., A.H., H.K., S.W., C.L., S.Y. and M.K. performed the experiments; M.I., T.W., M.H., S.C.D., M.O., K.S., G.Z., A.H., H.K., S.W., C.L., E.K., S.Y., M.K., Y.S., E.A.M., G.N. and Y.K. analysed the data; M.I., T.W., M.H., S.C.D., K.S., E.A.M., G.N. and Y.K. wrote the manuscript; M.I., T.W. and M.H. contributed equally to this work.

METHODS

Cells. Madin–Darby canine kidney (MDCK) cells and MDCK cells overexpressing Siaα2,6Gal (AX4 cells[17]) were maintained in Eagle's minimal essential medium (MEM) containing 5% newborn calf serum. Human embryonic kidney 293T cells were cultured in Dulbecco's modified Eagle's medium containing 10% fetal bovine serum (FBS). HeLa cells were maintained in MEM containing 10% FBS. All cells were maintained at 37 °C in 5% CO_2.

Plasmid construction and reverse genetics. Plasmid constructs for viral RNA production (pPolI)—containing the genes of the A/Vietnam/1203/2004 (H5N1; VN1203), A/Puerto Rico/8/34 (H1N1; PR8), A/Kawasaki/173/2001 (H1N1; K173) and A/California/04/2009 (H1N1; CA04) viruses flanked by the human RNA polymerase I promoter and the mouse RNA polymerase I terminator—were constructed as described[16]. The multibasic amino acids at the haemagglutinin (HA) cleavage site (RERRRKKR↓G) of the reassortant viruses between VN1203 and PR8 were changed to RETR↓G by site-directed mutagenesis. All transfectant viruses were generated by using reverse genetics essentially as described previously[16]. Recombinant viruses were amplified in MDCK or AX4[17] cells and stored at −80 °C until use. The HA segment of all viruses was sequenced to ensure the absence of unwanted mutations. All experiments with the reassortant viruses between VN1203 and CA04 were performed in enhanced biosafety level 3 containment laboratories approved for such use by the CDC and the USDA.

To introduce random mutations into the globular head of the VN1203 HA protein, a 143-amino-acid region spanning residues 120–259 (H3 numbering) was selected. This region was subjected to PCR-based random mutagenesis by use of the GeneMorph II kit (Stratagene) following the manufacturer's instructions. The targeted mutation rate (1–2 amino acid replacements per molecule) was achieved through optimization of the template quantity, and was confirmed by sequence analysis of 48 individual clones. By using a PCR-based cloning strategy, we inserted the mutagenized region into its respective vector containing the VN1203 HA gene between the human RNA polymerase I promoter and mouse RNA polymerase I terminator sequences. The composition of the plasmid library was confirmed by sequencing. The plasmid library was then used to generate an influenza virus library, essentially as described[16]. The size of the virus library was 7×10^6 p.f.u.

Preparation of sialidase-treated TRBCs. Turkey red blood cells (TRBCs) were washed three times with phosphate-buffered saline (PBS), and diluted to 20% (vol/vol) in PBS. TRBCs (1 ml) were incubated with 500 U of α2,3-sialidase from *Salmonella enterica* serovar Typhimurium LT2 (NEB) for 20–24 h at 37 °C, washed three times in PBS, and re-suspended in PBS or MEM containing 1% bovine serum albumin (BSA) (MEM/BSA).

Haemagglutination assay. Viruses (50 μl) were serially diluted with 50 μl of PBS in a microtitre plate. An equal volume (that is, 50 μl) of a 0.5% (vol/vol) TRBC suspension was added to each well. The plates were kept at room temperature and haemagglutination was assessed after a 1-h incubation.

Virus library screening. To select VN1203 HA variants that had acquired the ability to recognize human-type receptors, three parallel experiments were carried out, each with 0.7×10^6 viruses. The virus library was first incubated with 0.1 ml of 10% (vol/vol) α2,3-sialidase-treated TRBCs for 10 min at 4 °C. After this incubation, the TRBCs and bound viruses were pelleted at 1,000 r.p.m. for 1 min, and the pellets then washed ten times in MEM/BSA containing 313 mM NaCl. Bound viruses were eluted by incubation at 37 °C for 30 min and then diluted to approximately 0.5 virus per well (determined by virus titration in a pilot study). Individual viruses were then amplified in AX4 cells, which overexpress Siaα2,6Gal[17]. Individual viruses were re-screened by using haemagglutination assays with α2,3-sialidase-treated TRBCs.

Solid-phase binding assay. Viruses were grown in MDCK cells, clarified by low-speed centrifugation, laid over a cushion of 30% sucrose in PBS, and ultracentrifuged at 25,000 r.p.m. for 2 h at 4 °C. Virus stocks were aliquoted and stored at −80 °C. Virus concentrations were determined by using haemagglutination assays with 0.5% (vol/vol) TRBCs. The direct receptor-binding capacity of viruses was examined by use of a solid-phase binding assay as previously described[9]. Microtitre plates (Nunc) were incubated with the sodium salts of sialylglycopolymers (poly-L-glutamic acid backbones containing *N*-acetylneuraminic acid linked to galactose through either an α2,3 (Neu5Acα2,3Galβ1,4GlcNAcβ1-pAP) or an α2,6 (Neu5Acα2,6Galβ1,4GlcNAcβ1-pAP) bond) in PBS at 4 °C overnight. After the glycopolymer solution was removed, the plates were blocked with 0.15 ml of PBS containing 4% BSA at room temperature for 1 h. After four successive washes with ice-cold PBS, the plates were incubated in a solution containing influenza virus (8–32 HA units in PBS) at 4 °C overnight. After washing as described above, the plates were incubated for 2 h at 4 °C with rabbit polyclonal antiserum to either K173 or VN1203 virus. The plates were then washed again as before and incubated with horseradish peroxidase (HRP)-conjugated goat anti-rabbit IgG antiserum for 2 h at 4 °C. After washing, the plates were incubated with *O*-phenylenediamine (Sigma) in PBS containing 0.01% H_2O_2 for 10 min at room temperature, and the reaction was stopped with 0.05 ml of 1 M HCl. The optical density at 490 nm was determined in a plate reader (Infinite M1000; Tecan).

Virus binding to human airway tissues. Paraffin-embedded normal human trachea (US Biological) and lung (BioChain) tissue sections were deparaffinized and rehydrated. Sections were then blocked by using 4% BSA in PBS and covered with virus suspensions (64 HA units in PBS) at 4 °C overnight. After being washed four times in ice-cold PBS, the sections were incubated with primary antibodies for 3 h at 4 °C. The primary antibodies used were as follows: a pool of mouse anti-VN1203 HA monoclonal antibodies (15A3, 3G2, 7A11, 8A3, 14C5 and 18E1; Rockland); rabbit anti-K173 polyclonal antibody; rabbit anti-surfactant protein A polyclonal antibody (Millipore); and mouse anti-surfactant protein A monoclonal antibody (Abcam). Antibody binding was detected by using an IgG secondary antibody conjugated with Alexa Fluor 488 or Alexa Fluor 633 (Molecular Probes). Sections were also counterstained with Hoechst 33342, trihydrochloride, trihydrate (Molecular Probes). The samples were examined by using confocal laser scanning microscopy (model LSM 510; Carl Zeiss).

To confirm sialic-acid-specific virus binding, tissue sections were treated, before incubation with viruses, with *Arthrobacter ureafaciens* sialidase (Sigma) for 3 h at 37 °C. Viruses bound to tissue were detected as described above.

Experimental infection of ferrets. Animal studies were performed in accordance with the Animal Care and Use Committee guidelines of the University of Wisconsin-Madison. We used 6–10-month-old female ferrets (Triple F Farms) that were serologically negative by haemagglutination inhibition (HI) assay for currently circulating human influenza viruses. Six ferrets per group were anaesthetized intramuscularly with ketamine and xylazine (5–30 mg and 0.2–6 mg kg^{-1} of body weight, respectively) and inoculated intranasally with 10^6 p.f.u. (500 μl) of viruses. On days 3 and 6 after infection, three ferrets per group were killed for virological and pathological examinations. The virus titres in various organs were determined by use of plaque assays in MDCK cells.

Excised tissue samples of nasal turbinates, trachea, lungs, brain, liver, spleen, kidney and colon from euthanized ferrets were preserved in 10% phosphate-buffered formalin. Tissues were then trimmed and processed for paraffin embedding and cut into 5-μm-thick sections. One section from each tissue sample was stained by using a standard haematoxylin-and-eosin procedure, whereas another one was processed for immunohistological staining with a mixture of two anti-influenza virus rabbit antibodies (1:2,000; R309 and anti-VN1203; both prepared in our laboratory) that react with CA04 and VN1203, respectively. Specific antigen–antibody reactions were visualized by using an indirect two-step dextran-polymer technique (Dako EnVision system; Dako) and 3,3′ diaminobenzidine tetrahydrochloride staining (Dako).

Ferret transmission study. For transmission studies in ferrets, animals were housed in adjacent transmission cages that prevented direct and indirect contact between animals but allowed spread of influenza virus through the air (Showa Science; Supplementary Fig. 7). Three, five, or six ferrets were inoculated intranasally with 10^6 p.f.u. (500 μl) of virus (inoculated ferrets). Twenty-four hours after infection, three, five, or six naive ferrets were each placed in a cage adjacent to an inoculated ferret (contact ferrets). The ferrets were monitored for changes in body weight and the presence of clinical signs. To assess viral replication in nasal turbinates, we determined viral titres in nasal washes collected from virus-inoculated and contact ferrets on day 1 after inoculation or co-housing, respectively, and then every other day.

Serological tests. Serum samples were collected between days 14 and 20 after infection, treated with receptor-destroying enzyme, heat-inactivated at 56 °C for 30 min, and tested by use of an HI assay with 0.5% TRBCs (http://www.wpro.who.int/entity/emerging_diseases/documents/docs/manualonanimalaidiagnosisandsurveillance.pdf). Viruses bearing homologous HA were used as antigens for the HI tests.

Polykaryon formation representing membrane fusion activity. Monolayers of HeLa cells grown in 12-well plates were transfected with the protein expression vector pCAGGS[46] encoding wild-type or mutant HA. At 24 h after transfection, cells transiently expressing HA protein were treated with trypsin (1 μg ml^{-1}) in MEM containing 0.3% BSA for 30 min at 37 °C to cleave the HA into its HA1 and HA2 subunits. Polykaryon formation was induced by exposing the cells to low-pH buffer (145 mM NaCl, 20 mM sodium citrate (pH 6.0–5.4)) for 2 min at 37 °C. After this exposure, the low-pH buffer was replaced with MEM containing 10% FBS and the cells were incubated for 3 h at 37 °C. The cells were then fixed with methanol and stained with Giemsa's solution and photographed with a digital camera mounted on an inverted microscope (Nikon, Eclipse Ti). For quantitative analyses, cell nuclei were counted in five randomly chosen fields of cell culture. Polykaryon formation activity was calculated from the number of nuclei in polykaryons divided by the total number of nuclei in the same field.

Thermostability. Viruses (128 HA units in PBS) were incubated for the times indicated at 50 °C. Subsequently, infectivity and haemagglutination activity were determined by use of plaque assays in MDCK cells and haemagglutination assays using 0.5% TRBCs, respectively.

Neuraminidase (NA) inhibition assay. To assess the sensitivity of viruses to the NA inhibitor oseltamivir, NA inhibition assays were performed as described previously[32].

Statistical analysis. All statistical analyses were performed using JMP 9.0.0 (SAS Institute Inc.). The statistical significance of differences between rgCA04 and H5 avian/human reassortant viruses was determined by using a Dunnett's test. Comparisons of polykaryon formation between wild-type and mutant HAs were done using Tukey's test. P values of <0.05 were considered significant.

46. Niwa, H., Yamamura, K. & Miyazaki, J. Efficient selection for high-expression transfectants with a novel eukaryotic vector. *Gene* **108,** 193–199 (1991).

THE JOURNAL OF BIOLOGICAL CHEMISTRY VOL. 287, NO. 22, pp. 18182–18189, May 25, 2012

Signal Transducer and Activator of Transcription 3 (STAT3) Protein Suppresses Adenoma-to-carcinoma Transition in *Apc*$^{min/+}$ Mice via Regulation of Snail-1 (SNAI) Protein Stability*[S]

Received for publication, November 29, 2011, and in revised form, April 9, 2012 Published, JBC Papers in Press, April 10, 2012, DOI 10.1074/jbc.M111.328831

Jongdae Lee[1], **Joanna C. K. Kim, Shee-Eun Lee**[2], **Christine Quinley, HyeRi Kim, Scott Herdman, Maripat Corr, and Eyal Raz**[3]

From the Department of Medicine, University of California at San Diego, La Jolla, California 92093-0663

Background: STAT3 suppresses carcinogenesis of intestinal tumors in *Apc* min mice.
Results: STAT3 suppresses expression of SNAI in intestinal epithelium by regulating GSK3β activity.
Conclusion: STAT3 induces degradation of SNAI by promoting GSK3β activity and thereby suppresses adenoma-to-adenocarcinoma transition in *Apc* min mice.
Significance: Our data provide a new insight into the role of STAT3 in colorectal cancer biology.

STAT3 was recently reported to suppress tumor invasion in *Apc*$^{min/+}$ mice. We investigated the mechanisms by which STAT3 inhibits intestinal epithelial tumors using Apc$^{min/+}$/*Stat3*$^{IEC\text{-}KO}$ mice (intestinal epithelial cell (IEC)-specific deletion of STAT3 in the *Apc*$^{min/+}$ background) to determine the role of STAT3 in carcinogenesis *in vivo* as well as colorectal cancer cell lines *in vitro*. To inhibit invasion of IEC tumors, STAT3 functions as a molecular adaptor rather than a transcription factor. Accordingly, the tumors in *Apc*$^{min/+}$/*Stat3*$^{IEC\text{-}KO}$ mice undergo adenoma-to-carcinoma transition and acquire an invasive phenotype. Similarly, STAT3 knockdown in a colorectal cell line enhances IEC invasion. We demonstrate that STAT3 down-regulates SNAI (Snail-1) expression levels and hence suppresses epithelial-mesenchymal transition of colorectal cancer cells. Mechanistically, STAT3 facilitates glycogen synthase kinase (GSK) 3β-mediated degradation of SNAI by regulating phosphorylation of GSK3β. Our data identified a new role for STAT3 in the adenoma-to-carcinoma sequence of intestinal tumors.

STAT3 is a multifunctional transcription factor that is activated by various growth factors (*e.g.* epidermal growth factor and hepatocyte growth factor) and cytokines (*e.g.* IL-6 and IL-10). Consequently, STAT3 plays a key role in many biological processes such as cell growth, apoptosis, and inflammation (1). STAT3 is phosphorylated on a tyrosine residue (Tyr-705) by an upstream kinase JAK2 (Janus kinase 2). The phosphorylated protein forms either a homo- or heterodimer with other STAT proteins, then translocates to the nucleus and transcribes target genes. Rare nontranscriptional activities of STAT3 have also been reported. For example, STAT3 functions as an adaptor protein connecting IFNAR1 (interferon α receptor 1) and the p85 regulatory subunit of PI3K (phosphoinositide 3-kinase) (2), and it inhibits stathmin that depolymerizes microtubules (3). Recently, STAT3 was shown to inhibit intestinal epithelial cell (IEC)[4] tumor invasion in *Apc*$^{min/+}$ mice (4), but the underlying mechanisms remain unclear.

The development of human colon adenomas is initially induced by mutations in APC or β-catenin, and its transition to carcinoma is followed by sequential genetic mutations in K-Ras, SMAD2 or SMAD4, and p53. Whereas deletion of p53 does not provoke malignant transformation in *Apc*$^{min/+}$ mice (5), at least two genes were found critical for adenoma-to-adenocarcinoma transition. Tumors in *Smad4*$^{+/-}$/*Apc*$^{min/+}$ mice become malignant, showing an extensive stromal cell proliferation and submucosal invasion (6), and *Ephb3*$^{-/-}$/*Apc*$^{min/+}$ mice develop carcinomas that invade the muscle layer (7). However, the mechanisms by which these genes suppress IEC carcinogenesis are not fully understood.

The invasion of epithelial tumors to the surrounding tissues is associated with epithelial-mesenchymal transition (EMT), a process in which the epithelial tumor cells lose their epithelial phenotype and acquire a mesenchymal phenotype. Epithelial cells that have undergone EMT display reduced intercellular interactions but increased motility and invasiveness. Several transcriptional repressors were identified as inducers of EMT, including SNAI, Slug (Snail-2), E47, Twist, and the Zeb factors (8). Main targets of these proteins are cell adhesion molecules such as E-cadherin and claudins (CLDNs) that link epithelial cells together (8–11).

* This work was supported, in whole or in part, by National Institutes of Health Grants A1068685, A1095623, DK35108, and DK080506. This work was also supported by a grant from Crohns and Colitis Foundation of America.
[S] This article contains supplemental Figs. 1–3.
[1] To whom correspondence may be addressed: 9500 Gilman Dr., La Jolla, CA 92093-0663. Tel.: 858-822-5762; E-mail: j142lee@ucsd.edu.
[2] Present address: Dental Science Research Institute, Chonnam National University, 500-757 Gwangju, Korea.
[3] To whom correspondence may be addressed: 9500 Gilman Dr., La Jolla, CA 92093-0663. Tel.: 858-822-5762; E-mail: eraz@ucsd.edu.

[4] The abbreviations used are: IEC, intestinal epithelial cell; CA, constitutively active; CLDN, claudin; CRC, colorectal cancer; EMT, epithelial-mesenchymal transition; GSK3β, glycogen synthase kinase 3β; min, multiple intestinal neoplasia; MMP, matrix metalloproteinase; qPCR, quantitative PCR; SNAI, Snail-1; APC, adenomatous polyposis coli.

TABLE 1
PCR primers

Gene names	Forward primer	Reverse primer
h-*GAPDH*	5′-CAT GTT CGT CAT GGG TGT GAA CCA-3′	5′-AGT GAT GGC ATG GAC TGT GGT CAT-3′
h-*SNAI*	5′-TAC AGC GAG CTG CAG GAC TCT AAT-3′	5′-AGG ACA GAG TCC CAG ATG AGC ATT-3′

Glycogen synthase kinase 3β (GSK3β) performs multiple cellular functions (12). As an important regulator of metastasis, it suppresses the level of SNAI by being phosphorylated on two different sites: phosphorylation on the first site leads to ubiquitination and proteasomal degradation of SNAI whereas that on the second site controls the subcellular localization of SNAI (13). GSK3β is inactivated by phosphorylation by several different kinases at the Ser-9 residue (12, 14) but also can be regulated by phosphorylation at other residues: it is inactivated by phosphorylation at Thr-390 (15) and is activated by phosphorylation at Tyr-216 (16, 17). In addition, GSK3β activity is modulated by protein complex formation mediated by GSK3β-binding proteins and its subcellular localization (18). GSK3β is also a key regulator of β-catenin (19, 20), an effector molecule for the Wnt signaling pathway. Constitutive activation of β-catenin due to a mutation in the APC gene is the major cause of colorectal cancers (CRCs) (21) and induces the multiple intestinal neoplasia (min) phenotype in $Apc^{min/+}$ mice (21–23)

Here, we identified a novel adaptor function for STAT3 in IECs, which has a broad implication to CRC. Our data show that in a nontranscriptional fashion, STAT3 suppresses expression of SNAI, a major driving force in EMT and in the invasion of CRC cells. STAT3 interacts with GSK3β and negatively regulates phosphorylation of GSK3β, thereby inducing degradation of SNAI.

EXPERIMENTAL PROCEDURES

Reagents and Antibodies—Anti-STAT3, anti-β-catenin, anti-phospho-β-catenin, anti-GSK3β, anti-phospho-GSK3β (Ser-9), anti-SNAI, anti-Slug, anti-Zeb-1, anti-matrix metalloproteinase 7 (MMP7), anti-MMP9, and anti-E-cadherin antibodies were obtained from Cell Signaling Technologies (Danvers, MA). Anti-β-actin came from Sigma. Anti-ubiquitin, anti-MMP14, and anti-MMP15 antibodies were purchased from Santa Cruz Biotechnology (Santa Cruz, CA). Anti-claudin and anti-occludin antibodies were obtained from Lab Vision (Fremont, CA). Anti-vimentin and anti-fibronectin antibodies were obtained from BD Biosciences. Anti-axin antibody is from Invitrogen. The GFP-STAT3 plasmid was generously provided by Nancy C. Reich (24). Myc-GSK3β-CA plasmid (13) was obtained from Addgene (Cambridge MA). LiCl was obtained from Sigma and SB216763 from EMD Biosciences (Darmstadt, Germany).

Isolation of IECs from Mouse Intestines—Isolation was performed as described previously (25, 26).

Cell Culture—Culture conditions of IEC cells have been described previously (25). HCA-7 cells were cultured in low glucose DMEM, and HCT116 and RKO cells in high glucose DMEM (Mediatech, Manassas, VA).

Cell Invasion Assay—The cell invasion assay was performed with a basement membrane-coated CytoSelect™ 24-well cell invasion assay kit according to the manufacturer's instructions (Cell Biolabs, San Diego, CA). IECs (1×10^5 cells/well) were plated into each well 3 days after siRNA transfection and cultured for 2 days. The number of invaded cells per 4 high powered fields/well was visually counted using a microscope. The results are the average of two independent experiments, and the statistical analysis was performed by one-way ANOVA.

Quantitative PCR (qPCR), Immunoblotting, Immunohistochemistry, and Immunoprecipitation—These procedures were performed as described previously (25, 26). PCR primers are shown in Table 1.

Cell Proliferation Assay in Mice—Mice were administered BrdU intraperitoneally (2 mg/mouse) and killed 2 h after the injection. BrdU incorporation (proliferation) in paraffinized colonic tissues and the TUNEL assay in paraffinized colonic tissues were performed and analyzed according to the manufacturer's instructions (BD Biosciences).

siRNA-mediated Knockdown—Knockdown in IECs was performed with Nucleofector (Amaxa, Germany). Nontargeting siRNA #2 (luciferase targeting siRNA) from Dharmacon was used as a control. STAT3 siRNA (5′-CAACATGTCATTTGCTGAA-3′), GSK3β siRNA (5′-TCCGAGGAGAACCCAATGTTTCGTATA-3′), and SNAI siRNA (Applied Biosystems, Cat. No. s13186) were used.

Generation of $STAT3^{IEC\text{-}KO}$ Mice—To generate STAT3 deficiency specifically in IEC in mice, $Stat3^{flox/flox}$ mice (a gift from Shizou Akira, Osaka University, Osaka, Japan) were crossed to villin-Cre mice (on the C57BL/6J background; The Jackson Laboratory, Bar Harbor, ME), to create $Stat3^{IEC\text{-}KO}$ mice. Genotyping was performed as described (27). $Apc^{min/+}$ mice were obtained from The Jackson Laboratory. $Apc^{min/+}/Stat3^{IEC\text{-}KO}$ mice were generated by crossing $Apc^{min/+}$ mice with $Stat3^{IEC\text{-}KO}$ mice. All animal protocols received prior approval by the Institutional Animal Care and Use Committee.

RESULTS

STAT3 Suppresses Invasion of Intestinal Tumors in $Apc^{min/+}$ Mice—To determine the role of STAT3 in intestinal tumorigenesis, we conditionally deleted STAT3 in IEC ($STAT3^{IEC\text{-}KO}$) in $Apc^{min/+}$ mice (supplemental Fig. 1, *A* and *B*). At 20 weeks of age, the tumor count in $Apc^{min/+}/Stat3^{IEC\text{-}KO}$ mice was comparable with that in $Apc^{min/+}$ mice (supplemental Fig. 1*C*). In addition, proliferation of IECs in normal or tumor IEC was not significantly affected by STAT3 deletion (supplemental Fig. 1*D*).

Whereas the IEC tumors in $Apc^{min/+}$ mice were strictly confined to the mucosal crypts, those in the $Apc^{min/+}/Stat3^{IEC\text{-}KO}$ mice invaded the mucosal stroma, submucosa, and muscle (Fig. 1*A*). Such invasive tumors were found in all of the $Apc^{min/+}/Stat3^{IEC\text{-}KO}$ mice examined at 20 weeks ($n = 20$) of age and were confirmed by β-catenin immunostaining (Fig. 1*A*). At 25 weeks of age, the IEC tumors in $Apc^{min/+}/Stat3^{\Delta IEC}$ mice penetrated through the intestinal serosa (Fig. 1*B*). Although some of the

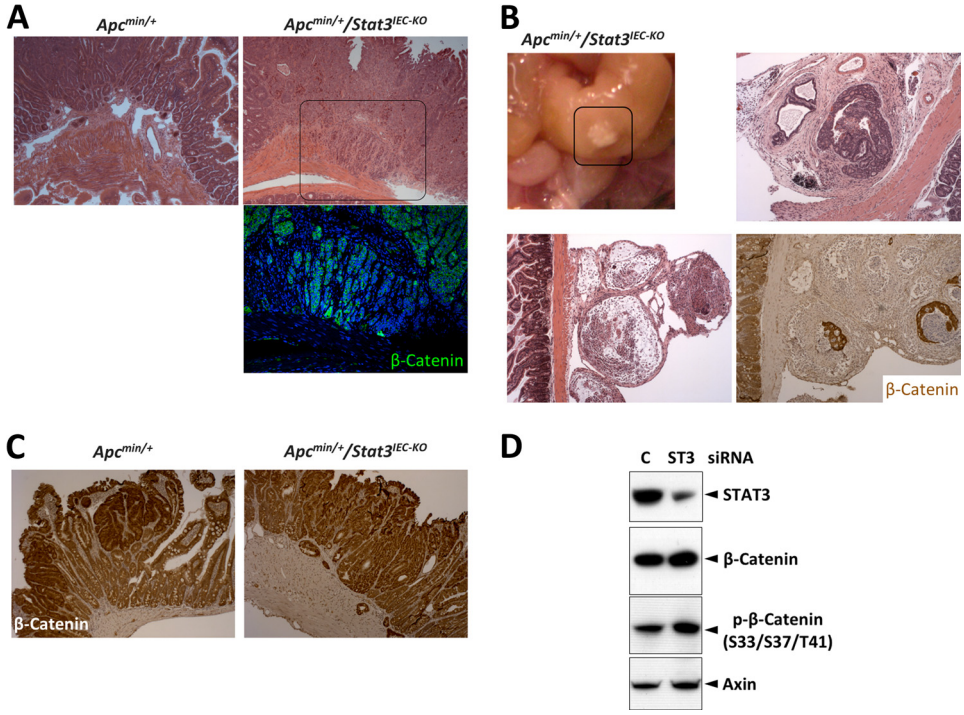

FIGURE 1. **STAT3 suppresses tumor invasion in *Apc*$^{min/+}$ mice.** *A*, deletion of STAT3^{IEC} induces invasion of tumors in *Apc*$^{min/+}$ mice. H&E (*upper panel*) and β-catenin (*lower panel*) staining of the small intestines shows the invasion of tumors in *Apc*$^{min/+}$/*Stat3*$^{IEC-KO}$ mice. *B*, tumors in *Apc*$^{min/+}$/*Stat3*$^{IEC-KO}$ mice penetrate the intestinal walls into the peritoneum. The *boxed area* in the *upper left panel* was analyzed by H&E and β-catenin staining. *C*, STAT3 does not regulate expression of β-catenin in *Apc*$^{min/+}$ mice. Expression of β-catenin in the small intestines was measured by immunohistochemistry. *D*, STAT3 suppresses activation of β-catenin in a CRC cell line. HCT116 cells were transfected with GFP or GFP-STAT3-WT (ST3), and the levels of the indicated proteins were measured by immunoblotting.

tumors penetrating serosa were necrotic, live tumor cells (β-catenin-positive) were also found surrounded by stromal tissues (Fig. 1*B*). However, STAT3 deletion did not significantly affect the levels of β-catenin in tumor cells (Fig. 1*C*). In a human colorectal cell line, STAT3 knockdown slightly enhanced the levels of β-catenin, phospho-β-catenin, and axin (a target of β-catenin), indicating that it can suppress the β-catenin pathway (Fig. 1*D*). Taken together, these findings validate that STAT3 in this animal model inhibits invasion of IEC tumors without affecting tumor induction (4).

STAT3 Suppresses EMT—Because EMT often precedes tumor invasion, we next investigated whether STAT3 deletion induces EMT in IEC tumors. Expression of E-cadherin or occludin was largely unaffected by STAT3 deletion (Fig. 2*A*), but expression of CLDN-3 and CLDN-5 was markedly decreased in tumor cells of *Apc*$^{min/+}$/*Stat3*$^{IEC-KO}$ mice compared with those in *Apc*$^{min/+}$ mice (Fig. 2*B*). Vimentin was expressed mainly in mesenchymal cells and rarely in tumor cells in *Apc*$^{min/+}$ mice; however, all of the tumor cells in the *Apc*$^{min/+}$/*Stat3*$^{IEC-KO}$ mice expressed vimentin at a high level (Fig. 2*C*). Fibronectin was also up-regulated in the tumor cells of *Apc*$^{min/+}$/*Stat3*$^{IEC-KO}$ mice whereas it was not detectable in tumor from *Apc*$^{min/+}$ mice (Fig. 2*D*). Interestingly fibronectin in *Apc*$^{min/+}$/*Stat3*$^{IEC-KO}$ was observed only in IEC tumor cells around the necrotic regions (Fig. 2*D*). Collectively, these data highly suggest that STAT3 suppresses EMT in IEC tumor cells in *Apc*$^{min/+}$ mice.

STAT3 Suppresses Expression of MMP14—We next checked the expression of MMPs, which are important for tumor invasion (28, 29). Whereas MMP7 expression in tumor cells was significantly lower in *Apc*$^{min/+}$/*Stat3*$^{IEC-KO}$ mice than that in *Apc*$^{min/+}$ mice, MMP9 or MMP15 (MT2-MMP) expression was minimal and observed mostly in nonepithelial cells in both strains of mice (supplemental Fig. 2). In contrast, MMP14 (MT1-MMP) expression in tumor cells was highly induced in *Apc*$^{min/+}$/*Stat3*$^{IEC-KO}$ mice but undetectable in *Apc*$^{min/+}$ mice (Fig. 2*E*). Interestingly, MMP14, a membrane type metalloproteinase, is particularly efficient in hydrolyzing basement membranes (30, 31), and its expression can be induced by SNAI in carcinomas (30).

STAT3 Suppresses Tumor Invasion via Down-regulation of SNAI—To examine further the suppressive effect of STAT3 on EMT, known regulators of EMT were examined. Whereas expression of Slug and Zeb-1 were barely detectable, and their levels were not significantly different in IEC tumor cells from both strains of mice (supplemental Fig. 3), SNAI expression was significantly elevated in *Apc*$^{min/+}$/*Stat3*$^{IEC-KO}$ tumor cells (Fig. 3*A*). To investigate further the role of STAT3 in SNAI expression and the role of SNAI in invasion, we used CRC cell lines in the subsequent studies. In three different CRC cell lines, HCT116, HCA-7, and RKO, STAT3 knockdown increased the expression of SNAI (Fig. 3*B*). Conversely, ectopic expression of STAT3-WT suppressed expression of SNAI (Fig. 3*C*).

We next tested whether the elevated SNAI was responsible for the invasive phenotype of STAT3-depleted CRC cells. STAT3, SNAI, or STAT3 with SNAI was silenced in HCT116 cells, and the transfected cells were subjected to an *in vitro* cell invasion assay. STAT3 knockdown significantly enhanced

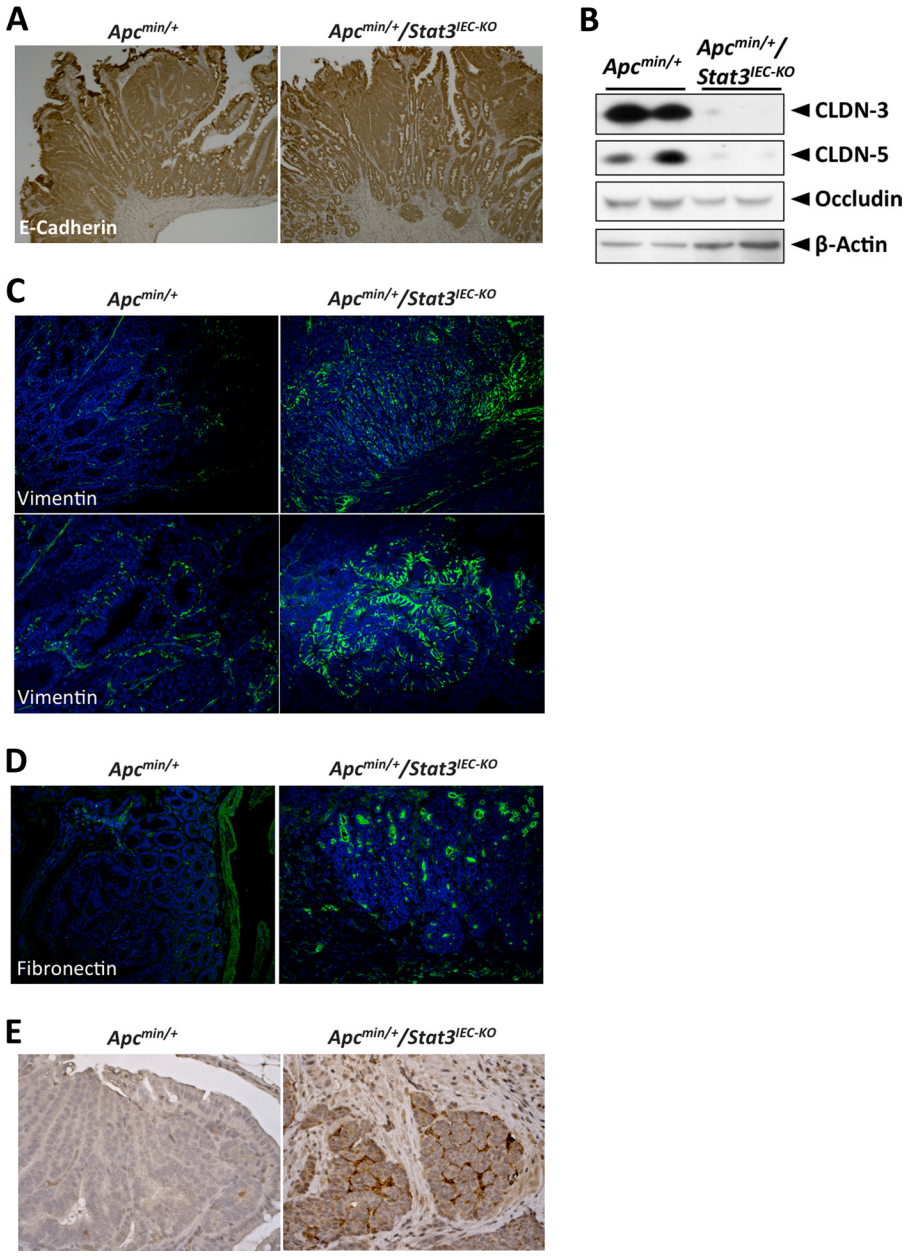

FIGURE 2. **STAT3 suppresses EMT in $Apc^{min/+}$ mice.** *A*, STAT3 does not regulate expression of E-cadherin in $Apc^{min/+}$ mice. Expression of E-cadherin in the small intestines was measured by immunohistochemistry. *B*, $STAT3^{IEC}$ maintains the expression of CLDNs in $Apc^{min/+}$ mice. Expression of the indicated proteins was measured by immunoblotting with the isolated tumor cells from the small intestines. *C*, STAT3 suppresses the expression of mesenchymal marker vimentin in $Apc^{min/+}$ mice. Expression of vimentin was measured by confocal imaging in the small intestines (*lower panel* original magnification, ×100). *D*, STAT3 suppresses the expression of mesenchymal marker fibronectin in $Apc^{min/+}$ mice. Expression of vimentin was measured by confocal imaging in the small intestines. Note that most of the fibronectin expression in $Apc^{min/+}/Stat3^{IEC\text{-}KO}$ mice is found in tumor cells around the necrotic regions. *E*, STAT3 suppresses the expression of MMP14 in $Apc^{min/+}$ mice. Expression of MMP14 was measured by immunohistochemistry in the small intestines.

invasiveness compared with control. In addition, SNAI knockdown alone or a combination of STAT3 and SNAI knockdown significantly curtailed the invasion (Fig. 3*D*). Thus, these data indicate that SNAI promotes invasion and that STAT3 down-regulates SNAI and thereby suppresses invasion of CRC cells.

STAT3 Promotes GSK3β Activity to Induce Degradation of SNAI—We next studied how STAT3 regulates SNAI expression. STAT3 deletion or knockdown in IEC did not significantly affect the transcription of SNAI (Fig. 4, *A* and *B*). We therefore examined whether STAT3 regulated SNAI via post-translational modification. SNAI in HCT116 cells was constitutively ubiquitinated and degraded by proteasomes (Fig. 4*C*). STAT3 knockdown significantly diminished the levels of SNAI ubiquitination, even though the levels of SNAI were higher than control (Fig. 4*C*). Because GSK3β phosphorylates SNAI, which leads to ubiquitination and proteasomal degradation (13), we investigated whether STAT3 is involved in the ubiquitin-mediated proteasomal degradation of SNAI via GSK3β. First, we found that GSK3β also down-regulates SNAI in CRC cell lines (Fig. 5*A*) and that inhibition of GSK3β activity with pharmacological inhibitors significantly increases SNAI (Fig. 5*B*). In addition, STAT3 forms a complex with GSK3β (Fig. 5*C*). Because

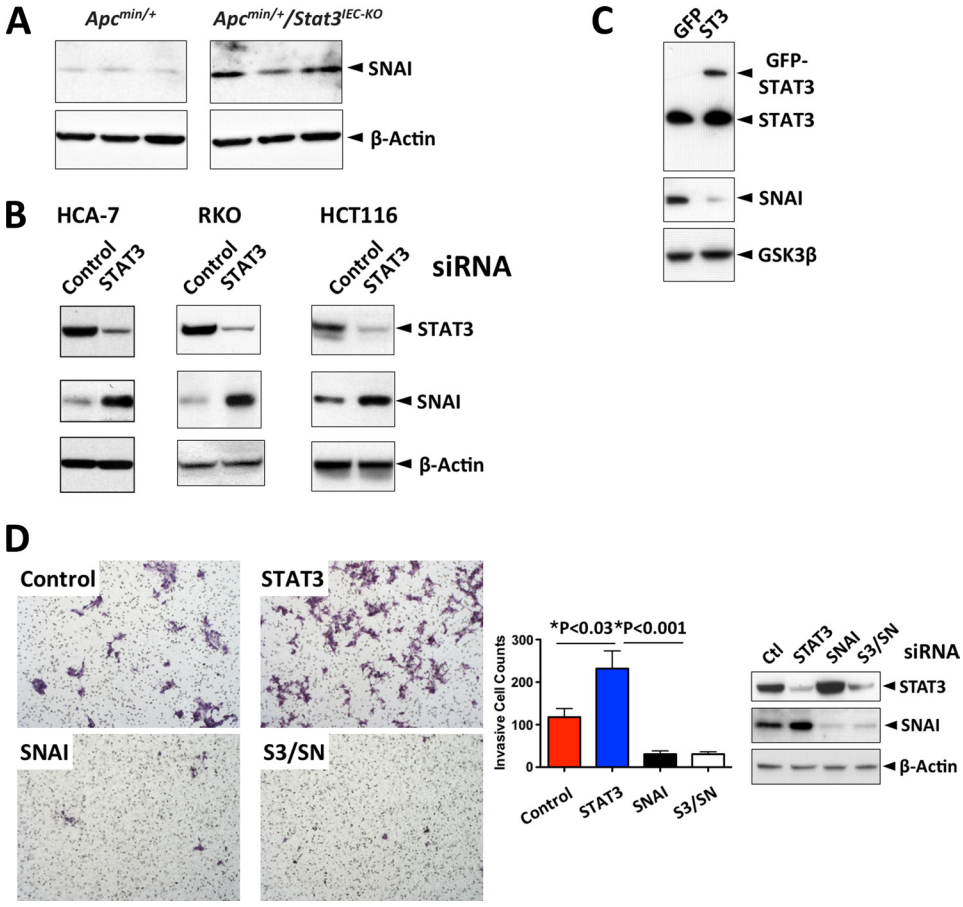

FIGURE 3. **STAT3 inhibits tumor invasion by suppressing expression of SNAI.** *A*, STAT3 suppresses expression of SNAI in $Apc^{min/+}$ mice. Expression of the indicated proteins was measured by immunoblotting from the isolated tumor cells from the small intestines. *B*, STAT3 suppresses expression of SNAI in human CRC lines. STAT3 was silenced by transfection of siRNA, and expression of the indicated proteins in the indicated CRC lines was measured by immunoblotting 3 days after transfection. *C*, STAT3 suppresses expression of SNAI in a human CRC cell line. HCT116 cells were transfected with either GFP or GFP-STAT3-WT, and the levels of the indicated proteins were measured by immunoblotting. *D*, SNAI mediates the invasion of the STAT3-depleted HCT116 cells. Cancer cell invasion assay was performed as described under "Experimental Procedures" 3 days after transfection of the indicated siRNA (*S3*, STAT3; *SN*, SNAI). The results are the average of two independent experiments ($n = 6$). The levels of the indicated proteins on the *bottom right* were measured by immunoblotting. *Error bars*, S.D.

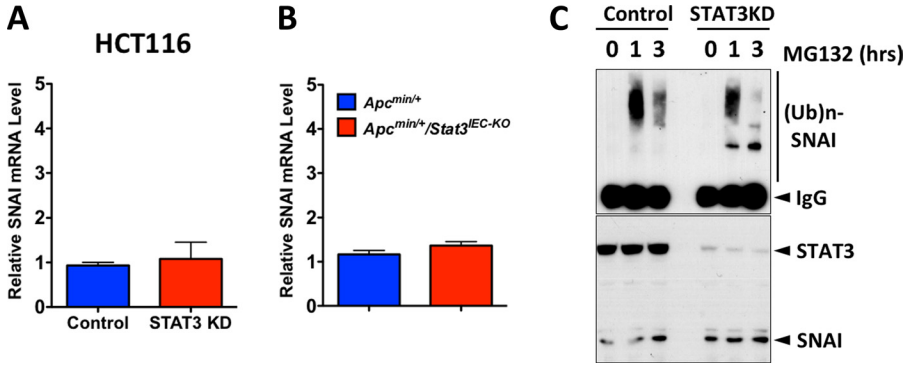

FIGURE 4. **STAT3 regulates SNAI at the post-transcriptional level.** *A*, STAT3 does not regulate transcription of SNAI. The mRNA levels of SNAI were measured by qPCR in HCT116 cells 3 days after siRNA transfection ($n = 4$). *B*, STAT3 does not regulate transcription of SNAI. The mRNA levels of SNAI were measured by qPCR in the indicated tumor cells ($n = 4$). *C*, STAT3 promotes ubiquitin-mediated degradation of SNAI in IECs. HCT116 cells were transfected with either control or STAT3 siRNA, treated with MG132 (10 μM) as indicated, SNAI was immunoprecipitated, and the gel was immunoblotted for ubiquitin (*upper panel* (*Ub*)*n*, polyubiquitin). The levels of STAT3 and SNAI were measured by immunoblotting (*lower panel*).

STAT3 deletion or knockdown did not significantly affect the expression of GSK3β (Fig. 5*C*), we examined whether STAT3 regulates activation (or phosphorylation) of GSK3β by Phos-tag SDS-PAGE (13, 32). Whereas there was no noticeable difference in GSK3β expression level between control and STAT3-deleted cells in a traditional SDS-PAGE analysis, the putative phosphorylated (retarded in mobility) GSK3β level was much higher in STAT3-deleted cells compared with that in control cells (Fig. 5*D*). STAT3 knockdown significantly increased the phosphorylation level on Ser9 residue of GSK3β (Fig. 5*E*). This result indicated that STAT3 negatively affects phosphorylation of GSK3β and suggested that STAT3 regu-

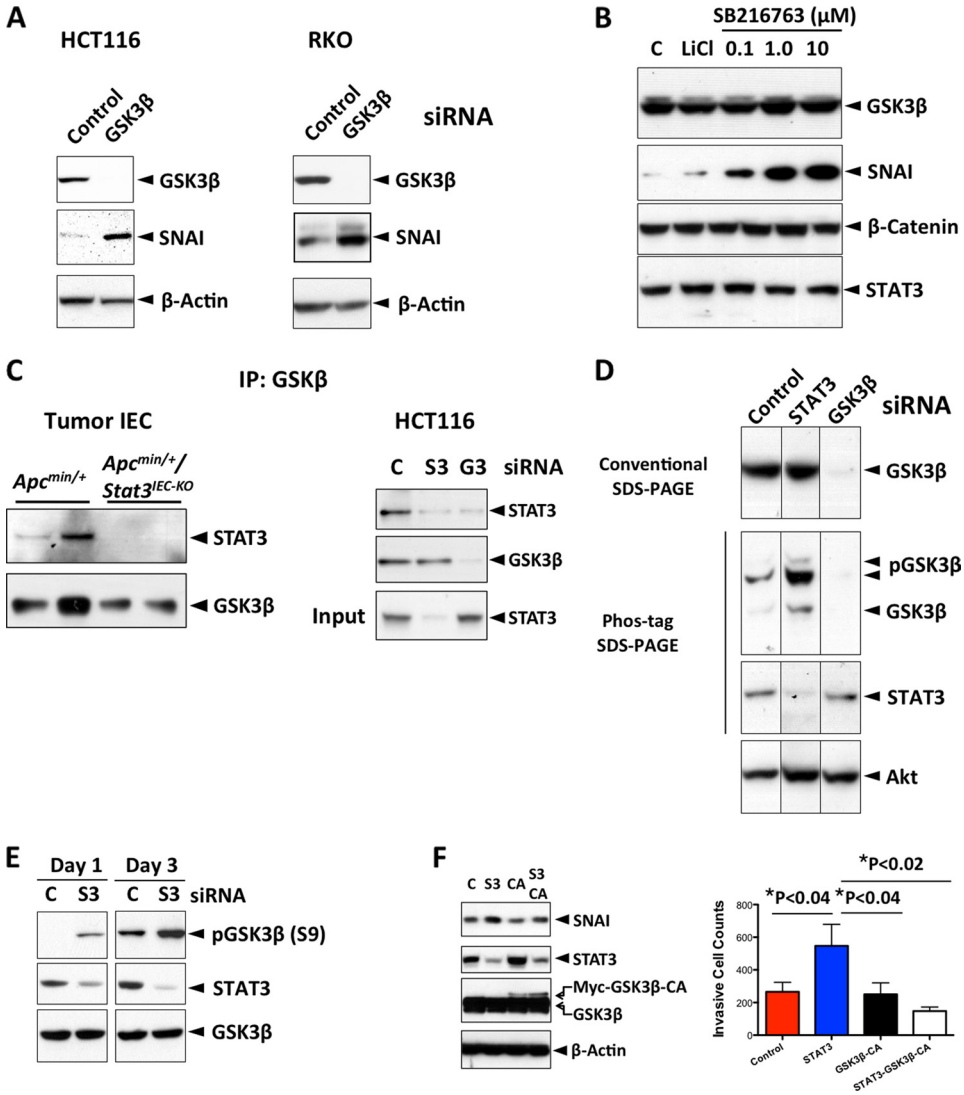

FIGURE 5. **STAT3 promotes GSK3β activity to induce degradation of SNAI.** *A*, GSK3β suppresses SNAI expression in CRC lines. The indicated protein levels were measured by immunoblotting 3 days after siRNA transfection. *B*, GSK3β suppresses SNAI via its kinase activity. HCT116 cells were treated with either LiCl (4 mM) or SB216763, GSK3β inhibitors as indicated for 4 h, and the indicated proteins were measured by immunoblotting. *C*, STAT3 interacts with GSK3β. GSK3β in isolated mouse tumor cells or in HCT116 cells was immunoprecipitated and immunoblotted for STAT3 (*S3*, STAT3; *G3*, GSK3β). *D*, STAT3 regulates phosphorylation levels of GSK3β. Lysates from HCT116 cells transfected with the indicated siRNA were divided and separated by either traditional SDS-PAGE or Phos-tag SDS-PAGE, and the indicated proteins were measured by immunoblotting. *E*, STAT3 inhibits phosphorylation at Ser-9 of GSK3β. HCT116 cells were transfected with the indicated siRNA (*C*, control; *S3*, STAT3), total cell lysates were collected 1 or 3 days after transfection, and the levels of indicated proteins were measured by immunoblotting. *F*, GSK3β-CA reverses the effects of STAT3 depletion. HCT116 cells were transfected with control siRNA (*C*), STAT3 siRNA (*S3*), GSK3β-CA plasmid, or STAT3 siRNA (*S3*) plus GSK3β-CA plasmid. Cell invasion assay ($n = 3$) and immunoblotting were performed 3 days after transfection.

lates SNAI expression and tumor invasion by promoting GSK3β activity. Therefore, we tested whether a constitutively active GSK3β (GSK3β-CA) mutant can reverse the effects of STAT3 depletion in HCT116 cells. Indeed, expression of GSK3β-CA reversed the increased SNAI expression and the increased invasiveness induced by STAT3 depletion (Fig. 5*F*). Taken together, these data provide evidence for a nontranscriptional and inhibitory role of STAT3 in IEC tumor invasion.

DISCUSSION

Although no naturally occurring mutations in STAT3 have been identified as a cause of any human cancer, it is considered as a strong promoter of carcinogenesis. STAT3 is activated in multiple solid and hematologic human malignancies, and its role in carcinogenesis has been validated in animal models (1, 33). For example, STAT3 was found to be crucial in initiation and progression of skin carcinoma (34), and the growth and survival of lymphomas are dependent on STAT3 (35). Recently, constitutively activating STAT3 mutations were identified in human hepatocellular adenomas, where the Tyr-640 mutant homodimerizes independently of upstream signals and is hypersensitive to IL-6 stimulation (36). In CRC, STAT3 activation (phosphorylation) was considerably up-regulated during adenoma-to-carcinoma progression (37, 38), but the precise role of STAT3 in CRC has not been yet defined.

Our data provide the mechanisms by which STAT3 suppresses tumor invasion both in an animal model and in CRC cell lines. STAT3 in IEC tumors of $Apc^{min/+}$ mice inhibits expression of an EMT inducer SNAI and mesenchymal markers, such as vimentin and fibronectin. Similarly, in CRC cell line

HCT116, STAT3 suppresses invasiveness by limiting expression of SNAI. Overexpression of a dominant negative STAT3 mutant in a CRC cell line was reported to cause down-regulation of E-cadherin (39). Although SNAI is widely known as a suppressor of E-cadherin, our data and another recent report (4) show that its expression is not significantly affected by STAT3 deletion in IEC. However, overexpression of SNAI did not suppress E-cadherin in a breast cancer cell line, whereas a mutant form (6SA) was able to do so (13). Therefore, it is possible that Ser-6 of SNAI may be phosphorylated in STAT3-deficient tumor cells.

Like STAT3, GSK3β is also a multifunctional protein involved in a wide range of physiological activities such as metabolism, cell development, and body pattern formation (12). It also plays a key role in Wnt signaling whose dysregulation is the most common cause of human CRC (2, 20). Our data show that STAT3 regulates GSK3β activity to control SNAI expression. We also found that STAT3 inhibits activation of β-catenin in a CRC cell line, but the mechanisms behind this phenomenon are yet to be investigated.

Interestingly, STAT3 in IECs is required for tumor induction in models of colitis-associated cancer. In colitis-associated cancer, STAT3 activation in IEC regulates cell survival and cell cycle progression through its transcriptional activation of downstream targets such as Bcl-X_L, c-Myc, and cyclin D1 (40–42). This colitis-associated cancer model employs a chemical mutagen, azoxymethane, and three cycles of the chemical irritant, dextran sodium sulfate, to induce colorectal tumors. Despite the observation that *Stat3*$^{IEC\text{-}KO}$ mice are much more susceptible to dextran sodium sulfate-induced colitis (41), it appears that STAT3 in IEC in *Apc* min model is necessary for their malignant transformation.

Overall, our data document the restraining role of STAT3 on the acquisition of an invasive phenotype of IEC tumors and explain the molecular basis that controls this process. We therefore propose that the inhibition of STAT3 in patients with CRC especially in advanced stages should be practiced with caution.

Acknowledgements—We thank Jennifer Meerloo for assistance in confocal imaging at the University of California at San Diego Neuroscience Microscopy Shared Facility funded by National Institutes of Health Grant P30 NS047101 through the NINDS.

REFERENCES

1. Yu, H., Pardoll, D., and Jove, R. (2009) STATs in cancer inflammation and immunity: a leading role for STAT3. *Nat. Rev. Cancer* **9,** 798–809
2. Pfeffer, L. M., Mullersman, J. E., Pfeffer, S. R., Murti, A., Shi, W., and Yang, C. H. (1997) STAT3 as an adapter to couple phosphatidylinositol 3-kinase to the IFNAR1 chain of the type I interferon receptor. *Science* **276,** 1418–1420
3. Ng, D. C., Lin, B. H., Lim, C. P., Huang, G., Zhang, T., Poli, V., and Cao, X. (2006) Stat3 regulates microtubules by antagonizing the depolymerization activity of stathmin. *J. Cell Biol.* **172,** 245–257
4. Musteanu, M., Blaas, L., Mair, M., Schlederer, M., Bilban, M., Tauber, S., Esterbauer, H., Mueller, M., Casanova, E., Kenner, L., Poli, V., and Eferl, R. (2010) Stat3 is a negative regulator of intestinal tumor progression in Apc(Min) mice. *Gastroenterology* **138,** 1003–1011.e1–5
5. Halberg, R. B., Katzung, D. S., Hoff, P. D., Moser, A. R., Cole, C. E., Lubet, R. A., Donehower, L. A., Jacoby, R. F., and Dove, W. F. (2000) Tumorigenesis in the multiple intestinal neoplasia mouse: redundancy of negative regulators and specificity of modifiers. *Proc. Natl. Acad. Sci. U.S.A.* **97,** 3461–3466
6. Takaku, K., Oshima, M., Miyoshi, H., Matsui, M., Seldin, M. F., and Taketo, M. M. (1998) Intestinal tumorigenesis in compound mutant mice of both *Dpc4* (*Smad4*) and *Apc* genes. *Cell* **92,** 645–656
7. Batlle, E., Bacani, J., Begthel, H., Jonkeer, S., Gregorieff, A., van de Born, M., Malats, N., Sancho, E., Boon, E., Pawson, T., Gallinger, S., Pals, S., and Clevers, H. (2005) EphB receptor activity suppresses colorectal cancer progression. *Nature* **435,** 1126–1130
8. Peinado, H., Olmeda, D., and Cano, A. (2007) Snail, Zeb, and bHLH factors in tumour progression: an alliance against the epithelial phenotype? *Nat. Rev. Cancer* **7,** 415–428
9. Carrozzino, F., Soulié, P., Huber, D., Mensi, N., Orci, L., Cano, A., Féraille, E., and Montesano, R. (2005) Inducible expression of Snail selectively increases paracellular ion permeability and differentially modulates tight junction proteins. *Am. J. Physiol. Cell Physiol.* **289,** C1002–1014
10. Ikenouchi, J., Matsuda, M., Furuse, M., and Tsukita, S. (2003) Regulation of tight junctions during the epithelium-mesenchyme transition: direct repression of the gene expression of claudins/occludin by Snail. *J. Cell Sci.* **116,** 1959–1967
11. Martínez-Estrada, O. M., Cullerés, A., Soriano, F. X., Peinado, H., Bolós, V., Martínez, F. O., Reina, M., Cano, A., Fabre, M., and Vilaró, S. (2006) The transcription factors Slug and Snail act as repressors of claudin-1 expression in epithelial cells. *Biochem. J.* **394,** 449–457
12. Plyte, S. E., Hughes, K., Nikolakaki, E., Pulverer, B. J., and Woodgett, J. R. (1992) Glycogen synthase kinase-3: functions in oncogenesis and development. *Biochim. Biophys. Acta* **1114,** 147–162
13. Zhou, B. P., Deng, J., Xia, W., Xu, J., Li, Y. M., Gunduz, M., and Hung, M. C. (2004) Dual regulation of Snail by GSK-3β-mediated phosphorylation in control of epithelial-mesenchymal transition. *Nat. Cell Biol.* **6,** 931–940
14. Cross, D. A., Alessi, D. R., Cohen, P., Andjelkovich, M., and Hemmings, B. A. (1995) Inhibition of glycogen synthase kinase-3 by insulin mediated by protein kinase B. *Nature* **378,** 785–789
15. Thornton, T. M., Pedraza-Alva, G., Deng, B., Wood, C. D., Aronshtam, A., Clements, J. L., Sabio, G., Davis, R. J., Matthews, D. E., Doble, B., and Rincon, M. (2008) Phosphorylation by p38 MAPK as an alternative pathway for GSK3β inactivation. *Science* **320,** 667–670
16. Hartigan, J. A., and Johnson, G. V. (1999) Transient increases in intracellular calcium result in prolonged site-selective increases in tau phosphorylation through a glycogen synthase kinase 3β-dependent pathway. *J. Biol. Chem.* **274,** 21395–21401
17. Lesort, M., Jope, R. S., and Johnson, G. V. (1999) Insulin transiently increases tau phosphorylation: involvement of glycogen synthase kinase-3β and Fyn tyrosine kinase. *J. Neurochem.* **72,** 576–584
18. Schaffer, B., Wiedau-Pazos, M., and Geschwind, D. H. (2003) Gene structure and alternative splicing of glycogen synthase kinase 3β (GSK-3β) in neural and non-neural tissues. *Gene* **302,** 73–81
19. Peifer, M., Pai, L. M., and Casey, M. (1994) Phosphorylation of the *Drosophila adherens* junction protein Armadillo: roles for wingless signal and zeste-white 3 kinase. *Dev. Biol.* **166,** 543–556
20. Yost, C., Torres, M., Miller, J. R., Huang, E., Kimelman, D., and Moon, R. T. (1996) The axis-inducing activity, stability, and subcellular distribution of β-catenin is regulated in *Xenopus* embryos by glycogen synthase kinase 3. *Genes Dev.* **10,** 1443–1454
21. Fearon, E. R. (2011) Molecular genetics of colorectal cancer. *Annu. Rev. Pathol.* **6,** 479–507
22. Bilger, A., Shoemaker, A. R., Gould, K. A., and Dove, W. F. (1996) Manipulation of the mouse germ line in the study of Min-induced neoplasia. *Semin. Cancer Biol.* **7,** 249–260
23. Fearon, E. R., and Vogelstein, B. (1990) A genetic model for colorectal tumorigenesis. *Cell* **61,** 759–767
24. Liu, L., McBride, K. M., and Reich, N. C. (2005) STAT3 nuclear import is independent of tyrosine phosphorylation and mediated by importin-α3. *Proc. Natl. Acad. Sci. U.S.A.* **102,** 8150–8155
25. Lee, J., Mo, J. H., Katakura, K., Alkalay, I., Rucker, A. N., Liu, Y. T., Lee, H. K., Shen, C., Cojocaru, G., Shenouda, S., Kagnoff, M., Eckmann, L.,

Ben-Neriah, Y., and Raz, E. (2006) Maintenance of colonic homeostasis by distinctive apical TLR9 signalling in intestinal epithelial cells. *Nat. Cell Biol.* **8,** 1327–1336
26. Lee, S. H., Hu, L. L., Gonzalez-Navajas, J., Seo, G. S., Shen, C., Brick, J., Herdman, S., Varki, N., Corr, M., Lee, J., and Raz, E. (2010) ERK activation drives intestinal tumorigenesis in *Apc*$^{min/+}$ mice. *Nat. Med.* **16,** 665–670
27. Kobayashi, M., Kweon, M. N., Kuwata, H., Schreiber, R. D., Kiyono, H., Takeda, K., and Akira, S. (2003) Toll-like receptor-dependent production of IL-12p40 causes chronic enterocolitis in myeloid cell-specific Stat3-deficient mice. *J. Clin. Invest.* **111,** 1297–1308
28. Kessenbrock, K., Plaks, V., and Werb, Z. (2010) Matrix metalloproteinases: regulators of the tumor microenvironment. *Cell* **141,** 52–67
29. Zucker, S., and Vacirca, J. (2004) Role of matrix metalloproteinases (MMPs) in colorectal cancer. *Cancer Metastasis Rev.* **23,** 101–117
30. Hotary, K. B., Allen, E. D., Brooks, P. C., Datta, N. S., Long, M. W., and Weiss, S. J. (2003) Membrane type I matrix metalloproteinase usurps tumor growth control imposed by the three-dimensional extracellular matrix. *Cell* **114,** 33–45
31. Ota, I., Li, X. Y., Hu, Y., and Weiss, S. J. (2009) Induction of a MT1-MMP and MT2-MMP-dependent basement membrane transmigration program in cancer cells by Snail1. *Proc. Natl. Acad. Sci. U.S.A.* **106,** 20318–20323
32. Kinoshita, E., and Kinoshita-Kikuta, E. (2011) Improved Phos-tag SDS-PAGE under neutral pH conditions for advanced protein phosphorylation profiling. *Proteomics* **11,** 319–323
33. Catlett-Falcone, R., Landowski, T. H., Oshiro, M. M., Turkson, J., Levitzki, A., Savino, R., Ciliberto, G., Moscinski, L., Fernández-Luna, J. L., Nuñez, G., Dalton, W. S., and Jove, R. (1999) Constitutive activation of Stat3 signaling confers resistance to apoptosis in human U266 myeloma cells. *Immunity* **10,** 105–115
34. Chan, K. S., Sano, S., Kiguchi, K., Anders, J., Komazawa, N., Takeda, J., and DiGiovanni, J. (2004) Disruption of Stat3 reveals a critical role in both the initiation and the promotion stages of epithelial carcinogenesis. *J. Clin. Invest.* **114,** 720–728
35. Chiarle, R., Simmons, W. J., Cai, H., Dhall, G., Zamo, A., Raz, R., Karras, J. G., Levy, D. E., and Inghirami, G. (2005) Stat3 is required for ALK-mediated lymphomutagenesis and provides a possible therapeutic target. *Nat. Med.* **11,** 623–629
36. Pilati, C., Amessou, M., Bihl, M. P., Balabaud, C., Nhieu, J. T., Paradis, V., Nault, J. C., Izard, T., Bioulac-Sage, P., Couchy, G., Poussin, K., and Zucman-Rossi, J. (2011) Somatic mutations activating STAT3 in human inflammatory hepatocellular adenomas. *J. Exp. Med.* **208,** 1359–1366
37. Kusaba, T., Nakayama, T., Yamazumi, K., Yakata, Y., Yoshizaki, A., Nagayasu, T., and Sekine, I. (2005) Expression of *p*-STAT3 in human colorectal adenocarcinoma and adenoma: correlation with clinicopathological factors. *J. Clin. Pathol.* **58,** 833–838
38. Park, J. K., Hong, R., Kim, K. J., Lee, T. B., and Lim, S. C. (2008) Significance of *p*-STAT3 expression in human colorectal adenocarcinoma. *Oncol. Rep.* **20,** 597–604
39. Rivat, C., De Wever, O., Bruyneel, E., Mareel, M., Gespach, C., and Attoub, S. (2004) Disruption of STAT3 signaling leads to tumor cell invasion through alterations of homotypic cell-cell adhesion complexes. *Oncogene* **23,** 3317–3327
40. Bollrath, J., Phesse, T. J., von Burstin, V. A., Putoczki, T., Bennecke, M., Bateman, T., Nebelsiek, T., Lundgren-May, T., Canli, O., Schwitalla, S., Matthews, V., Schmid, R. M., Kirchner, T., Arkan, M. C., Ernst, M., and Greten, F. R. (2009) gp130-mediated Stat3 activation in enterocytes regulates cell survival and cell cycle progression during colitis-associated tumorigenesis. *Cancer Cell* **15,** 91–102
41. Grivennikov, S., Karin, E., Terzic, J., Mucida, D., Yu, G. Y., Vallabhapurapu, S., Scheller, J., Rose-John, S., Cheroutre, H., Eckmann, L., and Karin, M. (2009) IL-6 and Stat3 are required for survival of intestinal epithelial cells and development of colitis-associated cancer. *Cancer Cell* **15,** 103–113
42. Grivennikov, S. I., and Karin, M. (2010) Dangerous liaisons: STAT3 and NF-κB collaboration and cross-talk in cancer. *Cytokine Growth Factor Rev.* **21,** 11–19